THE INTERACTION BETWEEN TECTONICS, TOPOGRAPHY, AND CLIMATE IN THE SAN JUAN MOUNTAINS, SOUTHWESTERN COLORADO

by

Ryan Edward McKeon

A thesis submitted in partial fulfillment
of the requirements for the degree

of

Master of Science

in

Earth Sciences

MONTANA STATE UNIVERSITY
Bozeman, Montana

January 2009

APPROVAL

of a thesis submitted by

Ryan Edward McKeon

This thesis has been read by each member of the thesis committee and has been found to be satisfactory regarding content, English usage, format, citation, bibliographic style, and consistency, and is ready for submission to the Division of Graduate Education.

Dr. David R. Lageson

Approved for the Department of Earth Sciences

Dr. Stephan G. Custer

Approved for the Division of Graduate Education

Dr. Carl A. Fox

STATEMENT OF PERMISSION TO USE

In presenting this thesis in partial fulfillment of the requirements for a master's degree at Montana State University, I agree that the Library shall make it available to borrowers under rules of the Library.

If I have indicated my intention to copyright this thesis by including a copyright notice page, copying is allowable only for scholarly purposes, consistent with "fair use" as prescribed in the U.S. Copyright Law. Requests for permission for extended quotation from or reproduction of this thesis in whole or in parts may be granted only by the copyright holder.

Ryan Edward McKeon

January 2009

ACKNOWLEDGEMENTS

I would like to begin by thanking my advisor David Lageson and my thesis committee members Cathy Whitlock and Bill Locke for guiding me through this project with many helpful conversations and suggestions along the way. Shari Kelley of New Mexico Tech graciously assisted me with my thermochronologic investigation, which would not have been possible otherwise. Eric Leonard of Colorado College is thanked for the use of his ELA data for the San Juans. In addition, I acknowledge the help of the following people: Ryan Bergstrom, Stuart Challender, Beth Helmke, Al Parker, and Colin Shaw.

I would also like to thank the following institutions for providing funding for this work:

The Colorado Scientific Society – William G. Pierce Memorial Fund

The American Alpine Club – Research Grant

The Wyoming Geological Association – J.D. Love Fellowship

Sigma Xi - Grant-in-Aid of Research # G20078231218196960

National Science Foundation – CREST Project to Shari Kelley

TABLE OF CONTENTS

LIST OF TABLES

Table Page

LIST OF FIGURES

Figure Page

ABSTRACT

Alpine glaciers have been referred to as ‘buzzsaws” on the grounds that they control the topographic development of actively deforming mountain ranges; however, the nature of the linkage between glacial erosion and topography in different tectonic and climatic settings remains unclear. In the San Juan Mountains of southwestern Colorado, an intracontinental mountain range with dramatically lower annual precipitation than previously studied ranges, distinct spatial variations in morphology resulting from Quaternary glaciation coincide with different exhumation histories that were derived using apatite (U-Th)/He thermochronology. The northwestern region had cooling ages of 3-10 Ma over an elevation range of 1300 m, moderate correlation between mean elevation and glacial thresholds, and regionally high values for relief and slope above cirque floors. The southern region, by contrast, had cooling ages of 19-32 Ma over an elevation range of 800 m, no correlation between mean elevation and glacial thresholds, and low values for relief and slope above cirque floors. The average magnitude of incision into a reconstructed maximum topography surface is nearly equal for the two study regions suggesting that the effects of glacial erosion are localized to high topography. The northwestern and southern regions show little variation in climate and fluvial and hillslope erosive potential, which implies that erosionally induced isostatic rebound is an unlikely source for the difference in cooling ages. Instead, I infer that active tectonism (possibly related to the Aspen anomaly) is responsible for different cooling ages and drove the greater degree of glacial modification of the northwestern region. As a result of the spatial variability in epeirogenic uplift, the San Juan Mountains appear to be both a mountain range that was just high enough to be glaciated, the southern region, and a mountain range where glacial erosion controls the elevation of high topography, the northwestern region; and thus are a microcosm for the diverse mountain ranges of the western United States.

INTRODUCTION

The onset of widespread alpine glaciation during the late Cenozoic as a result of global climate cooling has triggered much research into the linkage between climatic, erosive, and tectonic processes in orogenic belts. Whether the presence of high topography led to the change in climate (Raymo and Ruddiman, 1992) or a cooler climate and enhanced erosion led to higher topography (Molnar and England, 1990) is an ongoing question (e.g. Clift, 2006). Regardless, the striking coincidence of mountain peak elevation and glacial thresholds (Broeker and Denton, 1990) suggests the existence of a causal relationship between glacial erosion and topographic evolution of mountain ranges (Appendix A).

Comparative studies of the effects of fluvial and glacial erosion on topography have indicated that glacial processes enhance the volume of valleys and relief of ridges and peaks (Montgomery, 2002; Amerson et al., 2007) through flattening valley profiles and cirque headwall retreat (Brocklehurst and Whipple, 2002; Oskin and Burbank, 2005; Naylor and Gabet, 2007). Although the initial conversion of fluvially sculpted topography may lead to increases in relief, models of glacial erosion suggest a decrease of long wavelength relief in mountainous topography as a result of concentrated erosion high in tributary drainages and decreased erosion in sediment-choked trunk channels (Whipple et al., 1999; Tomkin and Braun, 2002) (Appendix A). In field studies from the Himalaya, southeast Alaska, Patagonia, and the Cascade Range (Brozovic et al., 1997; Montgomery et al., 2001; Spotila et al., 2004; Mitchell and Montgomery, 2006 respectively) the average height of actively deforming mountain ranges has been strongly

correlated with spatial variations in the regional glacier Equilibrium Line Altitude (ELA) irrespective of lithology or highly variable tectonic rock uplift rates. The highest erosion rates occur at the ELA where mass flux of the glacier is highest (Andrews, 1972; Tomkin and Braun, 2002, Berger and Spotila, 2008). Long-term glacial erosion at the ELA results in the formation of cirques over Quaternary timescales (Porter, 1989) (Appendix A). The relationship between mean elevation and ELA has led researchers to characterize glaciers as "buzzsaws", where glacial and periglacial processes control summit elevation above the ELA through enhanced erosion and the creation and maintenance of threshold slopes (Brozovic et al., 1997; Mitchell and Montgomery, 2006) (Appendix A).

The rate at which glaciers erode bedrock is highly variable and is dependent on ice sliding velocity, which is a function of mass flux (Hallet et al., 1996). Because of the large difference in precipitation (which controls accumulation and hence mass flux) between maritime and continental mountain ranges it is unlikely that all glaciated mountain ranges will reflect the topographic controls related to ELA as described by Brozovic et al. (1997). In the western United States, maximum elevation decreases systematically from south to north across the many isolated ranges of the Rocky Mountains, which coincides with decreasing Last Glacial Maximum (LGM) ELA (Porter et al., 1983) across the same area. The covariance of mountain peak elevation and ELA begs the question whether the Rocky Mountains were just high enough to support glaciation or whether glacial erosion has controlled the elevation of the Rocky Mountains. Mitchell and Montgomery (2006) contend that extensive glacial erosion has limited the elevation of the Cascade Range and Foster et al., (2008) suggest that small glaciers in the slowly uplifting mountain ranges of the northern Basin and Range

province of Idaho and Montana can efficiently control elevation, but has glaciation had the same effect on the other ranges of the western U.S? This study explores the impact of glacial erosion on the topographic evolution and exhumation history of the San Juan Mountains in southwestern Colorado in order to understand the role of glaciation in the development of intracontinental mountain ranges.

The San Juan Mountains have experienced extensive glaciation despite being located at the southeastern margin of alpine glacier accommodation in the Rocky Mountains during the Quaternary (Porter et al., 1983). Interestingly, the degree of modification to the landscape as a result of glacial erosion appears to be inconsistent across the range. The morphology of the San Juan Mountains is quite varied, encompassing landforms from high, flat, moderately dissected plateaus in the southern part of the range to spectacular rugged topography in the northwest (Figure 1). As a part of this study, an investigation into the variability of Neogene exhumation using low-temperature thermochronology indicates that the rugged topography of the northwestern San Juan Mountains correlates with younger cooling ages; however, the differential incision and exhumation could be driven by changes in climate or tectonic activity. Through a combination of thermochronologic and quantitative geomorphic techniques this study addresses the following questions: (i) can erosive processes explain differential exhumation between the northwestern and the southern San Juan Mountains? (ii) Do variations in climate or tectonic activity correlate with the degree of glacial modification and how do these differences impact the hypsometry of the area? (iii) Does the relationship between topography and glacial thresholds in the San Juan Mountains reflect a glacial buzzsaw effect?

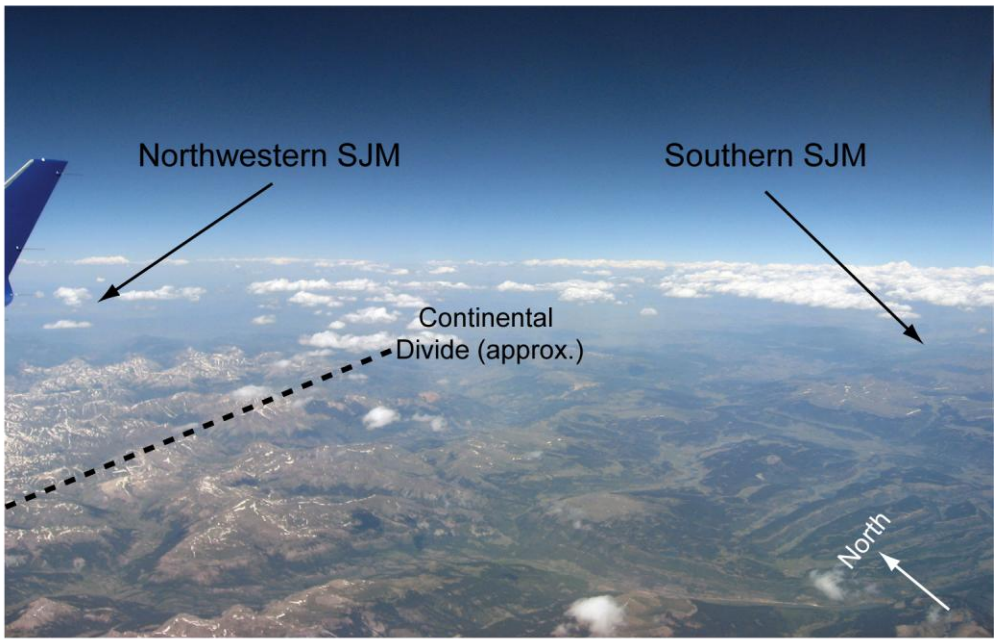

Figure 1. Photography taken from an airplane above the central San Juan Mountains by Eric Leonard. Note the difference in morphology between the left (Northwestern San Juan Mountains (SJM)) and the right (Southern San Juan Mountains).

STUDY AREA

With an average elevation in access of 3 km, the San Juan Mountains are a broad region of high topography within the southern Rocky Mountains located between the Colorado Plateau to the west and the Rio Grande Rift to the east (Figure 2). The majority of the range is composed of remnants of extensive Oligocene to early-Miocene volcanism related to the foundering of the subducted Farallon Plate beneath North America (Lipman et al., 1978). The intermediate volcanic rocks and associated sediments overlie the eastern margin of the Colorado Plateau, which outcrops as crystalline basement and Phanerozoic sedimentary cover in the southwest and western portion of the range (Figure 3). Faults in the area are related to massive caldera-forming eruptions and minor buoyant uplift and flow within a shallowly emplaced batholith beneath the range and have been inactive since the close of major volcanic activity at the beginning of the Miocene (Stevens and Lipman, 1976). Initiation of extension along the Rio Grande Rift coincided with the close of major volcanism and produced the asymmetric half graben of the San Luis Valley to the east of the San Juan

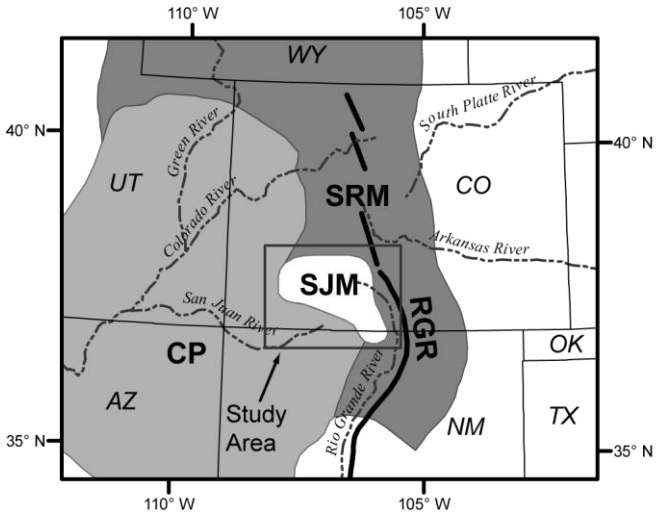

Figure 2. Map showing the location of the San Juan Mountains (SJM) at the boundary of the Colorado Plateau (CP), the Southern Rocky Mountains (SRM), and the Rio Grande Rift (RGR). Abbreviated state names and major rivers are included for reference. Adapted from McMillan et al. (2006).

Mountains resulting in the gentle eastward dip of volcanic units along the eastern flank of the range (Kellogg, 1999) (Figure 4).

The Continental Divide snakes through the radial drainage pattern of the range and separates the rugged and deeply dissected western portion from the more subdued and plateau-like eastern portion. After major volcanism ceased (ca. 26 Ma), little is known of the physiographic evolution of the San Juan region. Through examination of numerous outcrops of accordant ridgelines and flat expanses, Atwood and Mather (1932) mapped a peneplanation surface across the entire range and attributed the almost 2 km of vertical variation of the erosion surface to recent epeirogenic doming and incision of the area. With a greater understanding of the petrologic evolution of the San Juan volcanic field, Steven (1968) revisited the peneplain idea and concluded that the geologic relationships between outcrops of suspiciously flat ground did not support a temporally

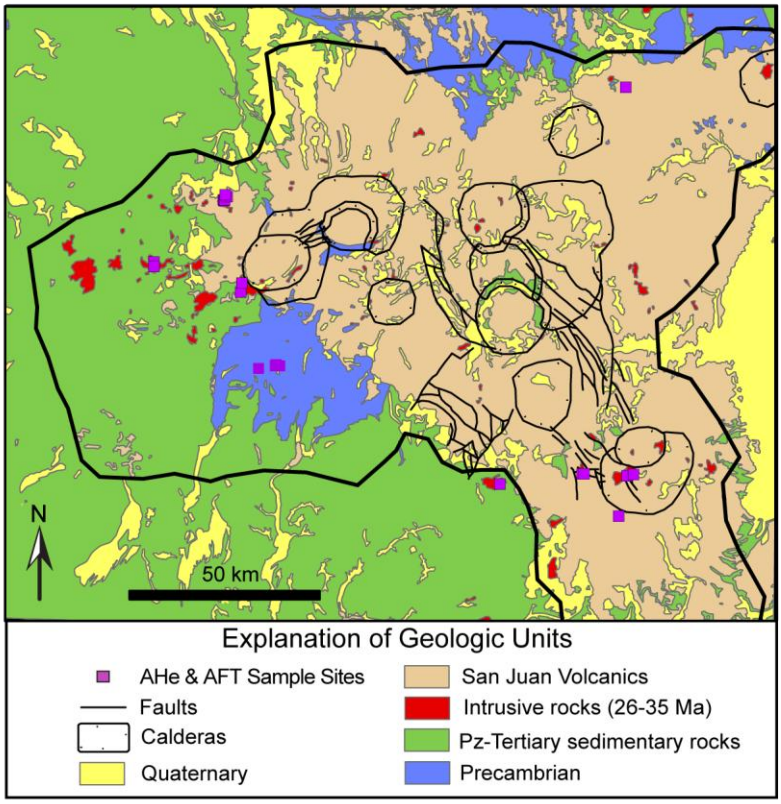

Figure 3. Generalized geologic map of the San Juan region (Green, 1992) with the location of thermochronologic (AHe and AFT) sample sites. The outline of the range front gives location reference from Figure 2. Caldera and fault locations are from Stevens and Lipman (1976).

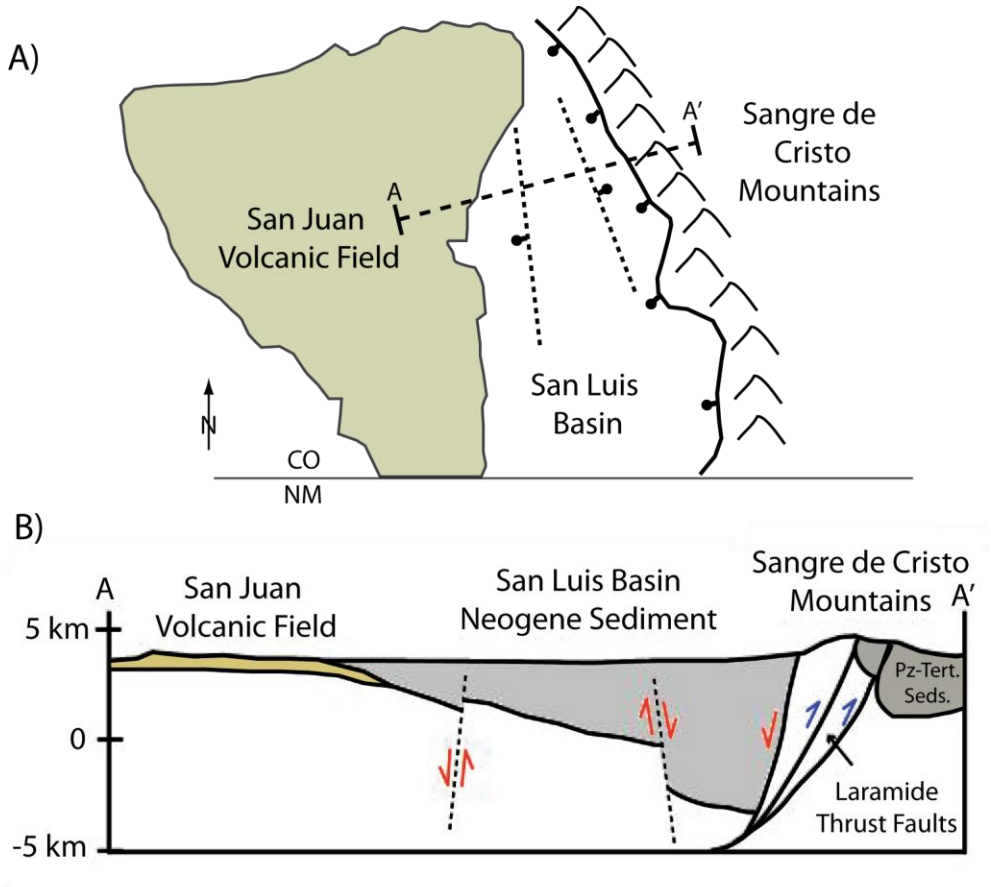

Figure 4. A) Map showing the location of the San Juan volcanic field, the San Luis Basin, and the Sangre de Cristo Mountains, with line A-A' indicating the location of the cross section in B. B) Schematic cross section from the San Juan volcanic field to the Sangre de Cristo Mountains after Kellogg (1999). Blue arrows indicate Laramide contractional faults and red arrow indicate Miocene-present extensional faults of the Rio Grande Rift.

coherent erosional origin. As a result of the work of Steven, the proposed San Juan peneplain, though a potentially useful datum for quantifying incision, is not considered in this study (Appendix B). Molnar and England (1990) cited paleobotanical evidence for negligible surface elevation change at Florissant in Central Colorado from the Eocene to present and proposed that the current rugged topography of the Colorado region could have been produced by an increase in of erosion and isostatic rebound as a result of global climate cooling. In contrast, many recent workers have concluded that the San

Juans specifically (Steven et al., 1995), and the Rocky Mountain Region as a whole (McMillan et al., 2006), have experienced some measure of late Cenozoic epeirogenic uplift and incision beginning ca. 6-8 Ma, however, the timing and mechanism has remained elusive. The actively extending Rio Grande Rift system to the east of the San Juan Mountains is a known area of high heat flow (Morgan et al., 1986) and may be source for regional uplift, however, the character of the asthenosphere underlying the rift has most recently been interpreted as a passive system (West et al., 2004) although the debate continues (e.g. Moucha et al., 2008). Alternatively, the source of regional uplift could be associated with the Aspen anomaly, a recently discovered region of low mantle velocities underlying central Colorado (Dueker et al., 2001, Karlstrom et al., 2005).

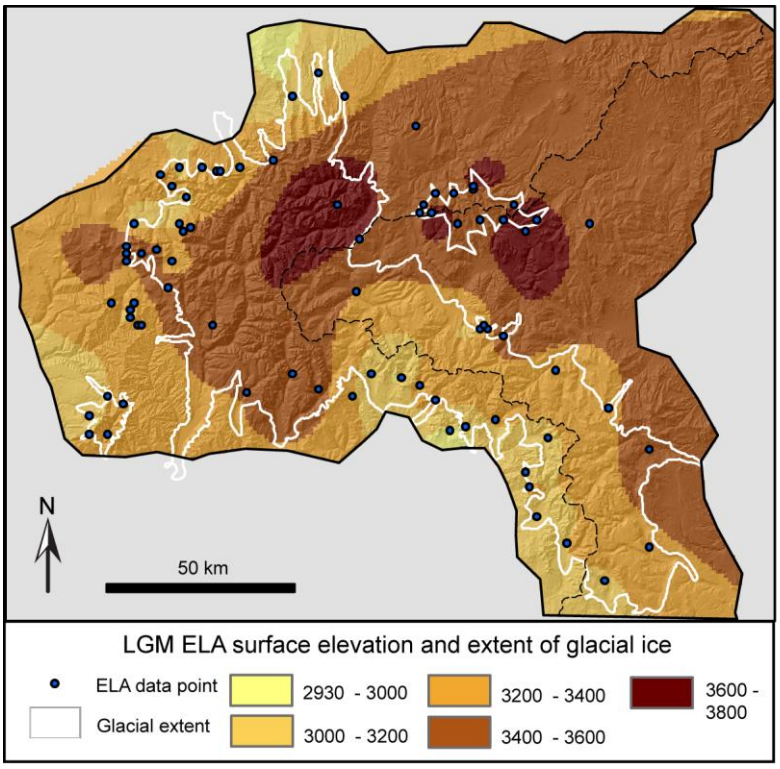

Figure 5. Map showing the extent of glacial ice (white line) during the Last Glacial Maximum (Atwood and Mather, 1932) and the spatial variation of ELA during the LGM (Leonard, 1984 and unpublished). The dashed line shows the location of the Continental Divide.

The modern San Juan Mountains support several small perennial snowfields but no alpine glaciers. Yet, the vast array of cirques and U-valleys attest to extensive

glaciation during the Quaternary. During the LGM, two ice cap-outlet glacier systems in addition to numerous cirque and valley glaciers covered approximately 5,000 km^2 (Atwood and Mather,1932; Leonard, 1984) (Figure 5). ELA gradients during the LGM were not substantially different from present precipitation gradients, suggesting that moisture circulation patterns have not changed from the LGM to present (Leonard, 1984).

The southwestern U.S. shows a distinct seasonal variation in the amount and distribution of precipitation (Mock, 1996) that is related to annual changes atmospheric circulation. Presently and during the LGM, the source of winter moisture is form the west-northwest from the Pacific Ocean (Bartlein et al., 1998; Sheppard et al., 2002). During the summer the San Juan Mountains are likely influenced by monsoonal flow from the southwest, however the extent to which this overprints the dominantly western jet stream is unclear (e.g. Sheppard et al., 2002). Monthly precipitation data form 19 SNOTEL (SNOwpack TELemetry) sites throughout the San Juan Mountains show that there is little spatial variation in the seasonality of

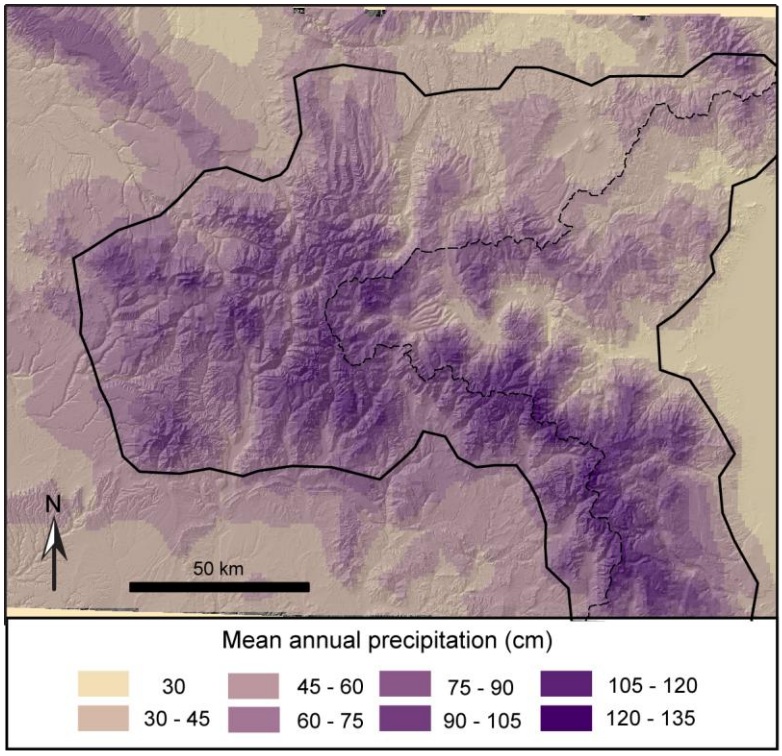

Figure 6. Map showing mean annual precipitation for the San Juan Mountains. Data provided by the PRISM Group. The dashed line indicates the location of the Continental Divide.

precipitation maxima and minima within the range. Spring and early summer are the wettest months in the San Juan region and September is by far the driest month throughout the area. (Appendix B). Modeled annual precipitation estimates from the PRISM Group (Oregon State University, http://www.prism.oregonstate.edu) incorporate SNOTEL data and reflect a western moisture source and orographic control (Figure 6), with maximum precipitation (~100 – 135 cm/yr) concentrated near the Continental Divide and minimum precipitation (~50 cm/yr) in the northeastern part of the range.

METHODS

The morphological contrast between the rugged northwestern and more subdued southern portions of the San Juan Mountains presents an ideal location to investigate how glacial erosion has impacted topographic development and potentially what is driving the differing degrees of glacial modification within a single mountain range. To accomplish this, low-temperature thermochronology was used to analyze the spatial variation of cooling history in the San Juan Mountains. In addition, ArcGIS software was used to: 1) quantify differences in topographic and climatic characteristics between the northwestern and southern regions; 2) estimate average Quaternary ELA from cirque elevation and analyze cirque morphology; 3) create topographic swath profiles for each region to compare with tends in ELA, precipitation, and exhumation; 4) model the distribution and magnitude of incision in both regions; and 5) apply two different erosion models to understand the potential connection between erosion and exhumation.

Apatite Thermochronology

Spatial variations in the low-temperature cooling history of the San Juan region were investigated with apatite (U-Th)/He (AHe) and fission-track (AFT) thermochronologic techniques. These techniques were chosen for their low closure temperatures, ~70°C for (U-Th)/He (Farley, 2000) and ~110°C for fission-track (Laslett et al., 1987; Ketcham et al., 1999), which makes them sensitive to small-magnitude exhumation from several kilometers depth (Ehlers and Farley, 2003) (Appendix C). For clarification, terminology surrounding uplift and erosion follows the definitions of

Molnar and England (1990), wherein rock uplift is the upward movement of a parcel of rock relative to a datum, surface uplift is rock uplift minus exhumation, exhumation is the thickness of rock removed through tectonic or erosive processes, and the cooling age is the duration of time elapsed during the transport of a parcel of rock from the depth of the closure temperature to the surface.

To ensure that the rocks sampled crystallized at a higher temperature than the closure temperature for the apatite (U-Th)/He system, samples were collected from coarse crystalline intrusions that were emplaced during the Oligocene. Outcrop of intrusive igneous rock is restricted to the northwestern and southern regions of the San Juan Mountains, which served not only to focus the exhumation investigation, but also the landscape analysis to these two regions (Figure 7). To clarify future references to location, the northwestern San Juan Mountains refers to the area surrounding the three AHe and one AFT sample sites in the northwestern portion of the range, henceforth referred to as "NW-SJM"; similarly, the southern San Juan Mountains refers to the area surrounding the three AHe sample sites in the southern portion of the range, henceforth referred to as

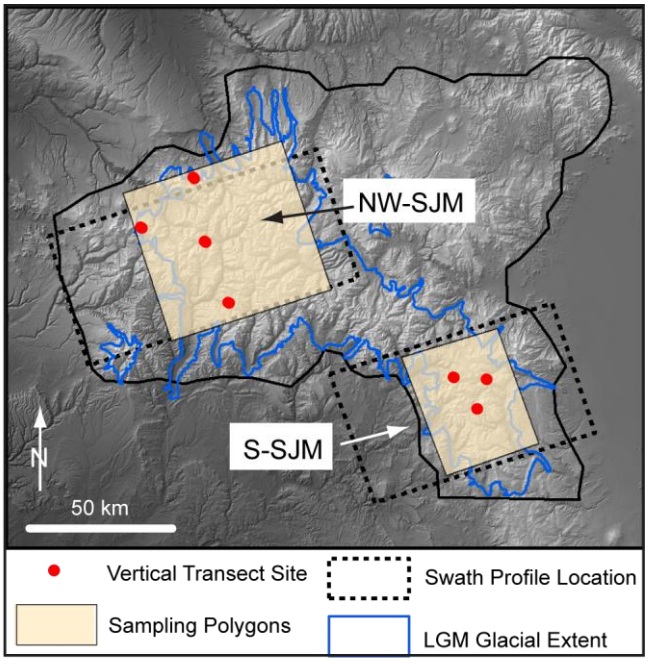

Figure 7. Map showing the location of the sampling polygons used for topographic and climatic parameters for the northwestern (NW-SJM) and southern (S-SJM) study regions along with the boundaries of the swath profile analysis (dashed rectangles).

"S-SJM" (Figure 7). Individual intrusions were selected in each area to avoid locally extensive hydrothermal alteration and to maximize the vertical exposure of suitable rock. Samples were collected along vertical transects, such that multiple samples from different elevations from each intrusion were colllected to best constrain the history of cooling as a result of exhumation.

Of 25 samples collected from six intrusions, 16 had apatite grains that were of suitable purity, form, and size for single-grain analysis, which was carried out at the (U-Th)/He Laboratory at the University of Kansas. Because the presence of tiny inclusions was common in these samples, ages were calculated using single-grain aliquots. Ages are reported as the mean of three single-grain ages for each sample (± 6% analytical error, 2σ) (see Appendix C for more information). AFT ages from six samples were derived from Precambrian crystalline rocks of the Needle Mountains in the NW-SJM (collected and analyzed by Dr. Kelley at NM Tech).

Topographic and Climatic Characteristics

To understand how variations in climate or tectonics drove the observed difference in morphology and glacial modification between the NW-SJM and S-SJM, a comparison of topographic and climatic characteristics was conducted as a base for more detailed investigations to build on. The zone boundaries for this analysis (and subsequent analyses where indicated) were created to be centered on the thermochronology sample sites and encompass the highest topography and glaciated area of each region (Figure 7) (Appendix C). Topographic data was derived from a 30-m USGS Digital Elevation Model (DEM) from the National Elevation Dataset (http://ned.usgs.gov) from which the

means of modern elevation and relief of each zone were calculated. Relief for each cell within a zone was calculated as the difference between the maximum and minimum elevation within a sampling window with a radius of 2 km. The size of the window was chosen to be large enough to capture the area of tributary drainages, but small enough so as not to sample topography from different ridgelines across larger valleys. Mean annual precipitation data was sampled from a 30-year average (1961-1990) obtained from the PRISM Group at Oregon State University; this data is an estimation of the mean annual spatial distribution of precipitation using point measurements measured at SNOTEL sites and an orographic precipitation model (Daly et al., 2002). The mean of LGM ELA for the northwestern and southern San Juans was derived from a spline surface generated using ELA estimates of 78 glaciers from Leonard (1984 and unpublished) (Appendix C) that were calculated using the Accumulation Area Ratio method.

Cirque Analysis

U-shaped valleys, arête ridges, and cirques are the product of repeated glaciations spanning the Quaternary. Therefore, the LGM ELA represents only the most recent snapshot of this longer climate signal. Porter (1989) recognized this limitation and suggested that the elevation of the outlets of cirques could be used to approximate the average Quaternary ELA. Mitchell and Montgomery (2006) decribe a relatively easy process to calculate the spatial variation in Quaternary average ELA and analyze its impact on topography in their study of the Cascade Range from which was used in this study. It should be noted that because there are no modern glaciers in the San Juan

Mountains from which to measure the change in ELA from past to present, any estimation will represent a minimum bound for the actual amount of change.

From Digital Raster Graphics (DRGs) of 7.5-minute USGS topographic maps (obtained from the GIS Database of the Mountain Studies Institute http://www.mountainstudies.org), the outlets of northeast-facing cirques (0-90° from north) were identified and their elevations extracted from a DEM (Figure 8) for the NW-

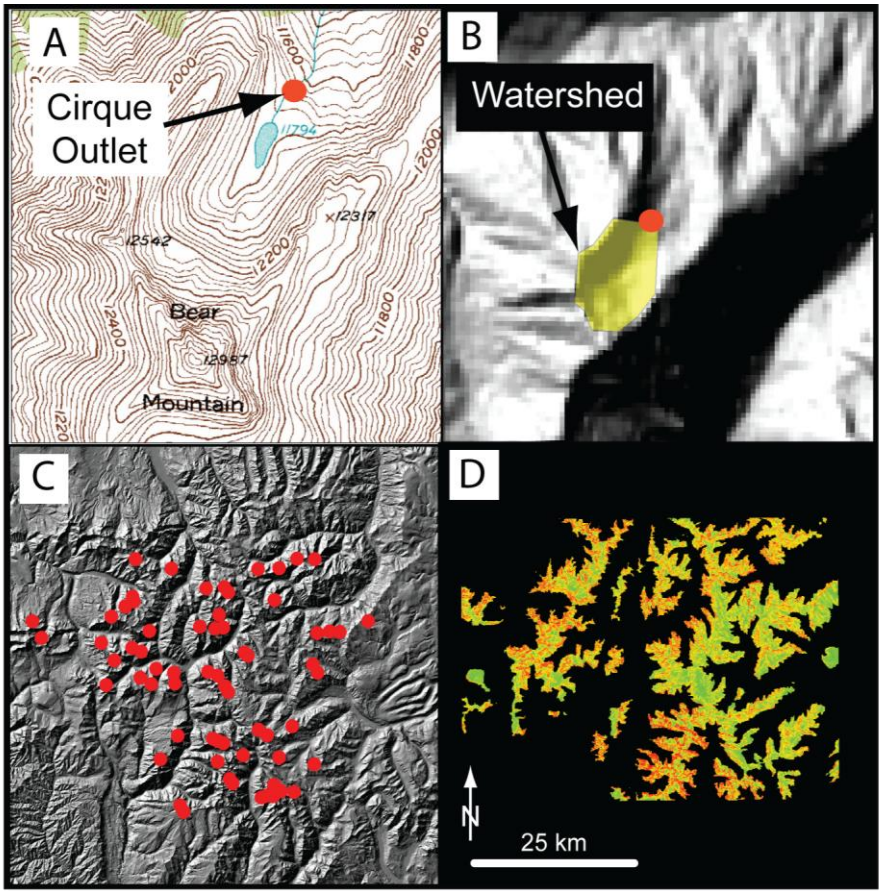

Figure 8. Steps for cirque morphology analysis adapted from Mitchell and Montgomery (2006) A) Cirque outlet locations determined from USGS Digitized topographic Quads. B) Watersheds used to measure relief. C) The distribution and elevation of cirque outlets was used to create a third order polynomial surface representing average Quaternary ELA (Porter, 1989). D) Slope was measured for topography that stands above the average Quaternary ELA.

SJM and S-SJM. Only northeast-facing cirques were used in order to control for climatic variability associated with the timing and duration of solar radiation on different sides of a mountain ridge (e.g. Humlum, 1986). With a flow-routing algorithm, watersheds were created to measure relief for each cirque outlet. The change in elevation from the cirque outlet to the highest point in the catchment defines the cirque relief. Because of the inaccuracy of watershed boundaries created using ArcGIS in the flatter topography of the S-SJM, the average slope above cirque floors for both regions was measured by isolating all topography above a best-fit third-order average Quaternary ELA surface that was generated for the San Juan Mountains. The third-order surface was chosen as a balance between minimizing both the root mean square deviation and the degrees of freedom, thus accurately portraying the data while keeping the complexity low. Slope was calculated by fitting a 3 X 3 grid around each cell in a DEM of the range and using the change in elevation between neighboring cells to calculate a slope angle for the target cell.

Topographic Swath Profiles

To analyze the spatial correlation between topography and various climate parameters, 50 km wide topographic swath profiles were created for the NW-SJM and S-SJM (Figure 7). Swath profiles were produced using DEMs in conjunction with a Matlab script written by Eric Kirby of Pennsylvania State University. The location and orientation of the swath profiles was based on sampling topography parallel to the direction of the prevailing winds, thus analyzing the topographic response to orographic precipitation gradients. The mean and maximum elevation across each region was

calculated to compare topography with gradients in modern precipitation, LGM ELA, and average Quaternary ELA. Quantitative analysis of the correlation between topography and average Quaternary ELA was accomplished by sampling the different parameters at 1 km intervals across the swath profiles.

Erosion Models

As the current unglaciated state of the range would suggest, the impact of glacial erosion on the topography and exhumation history of the San Juans requires an understanding of the effect of non-glacial erosive processes. To this end, simple models of fluvial and hillslope erosion potential were applied to the study regions to determine if functional differences in non-glacial erosion potential could explain the variation in morphology that is evident in the field. To address this question I follow the methods outlined by Mitchell and Montgomery (2006) to produce models the of stream power and hillslope erosion: A stream power model from Bagnold (1960) was use to quantify the energy expenditure per unit channel length:

$$\Omega = \rho g Q S \qquad (1)$$

where Ω is stream power, ρ is the density of water (1000 g m^{-3}), g is the acceleration due to gravity (9.8 m s^{-2}), and S is a unitless measure of slope. Because annual precipitation in mountainous terrain is variable, a simple approximation of discharge based on the contributing area alone can be misleading. In my model, discharge (Q) was calculated by weighting each cell in a watershed based on its mean annual precipitation and then using a flow-routing algorithm to generate a flow network using the weighed cells. As explained by Mitchell and Montgomery (2006), this approach assumes that all

precipitation that falls annually in a given cell turns into runoff and ignores the influence of seasonal or storm variability on precipitation phase and intensity. In addition, different lithologies and preexisting structural fabrics in bedrock can impact rates of fluvial erosion and as a result this model describes only the long-term erosion potential of different regions of the San Juan Mountains. In order to isolate the channels where fluvial erosion occurs, the average stream power was calculated by removing all values where $\Omega < 1.0 \times 10^9$ because these values are characteristic of contributing cells that are not part of a stream channel and as such are not a good representation of fluvial erosive processes. Hillslope erosion potential was modeled using the product of slope and annual precipitation on a per cell basis that differs from the stream power model because every cell is a unique approximation of the forces acting upon it. This model assumes that areas characterized by steeper and/or wetter conditions are more susceptible to hillslope processes, such as discrete events like landslides and debris flows, as well as ongoing processes of creep and rainsplash. A model of glacial erosion was not undertaken for the San Juans due to the complexity of modeling such processes (e.g. Tomkin and Braun, 2002).

The results of the erosion models were sampled in two ways. First, to address whether fluvial or hillslope processes exert a control on exhumation, the maximum stream power and mean hillslope potential was calculated within a 5-km-radius sampling window centered on each thermochronologic sample site. If either process were responsible for controlling exhumation, than one would expect areas of higher erosive potential to coinside with younger cooling ages signaling extensive recent exhumation. The radius was chosen to be large enough to capture the channel that drains the area

where the sample was collected, thus measuring the maximum fluvial potential in the sample area, as well as to account for variation in hillslope erosion potential caused by the local presence of cliffs, cirques, and tarns. The second sampling technique was broader in scale and meant to address fundamental differences in erosive potential between the study regions. The average for both erosion models were calculated within the zone polygons for each region from the first analysis of topography and climatic parameters (Figure 7).

Incision and Isostatic Rebound

The analysis of cirque morphology allows comparison of the glacial modification between the NW-SJM and S-SJM. The erosion models identify similarities or differences in fluvial and hillslope erosion potential, but, to understand how erosion as a whole has impacted the topographic development and exhumation history of the San Juan Mountains, it is necessary to quantify the distribution and magnitude of geophysical relief. Small and Anderson (1998) introduced the measurement of geophysical relief or elevation change from a pre-incision surface to the modern valley floor to quantify the amount of mass removed from an area and calculate the resulting isostatic uplift. Because of the coupling of erosion and isostatic rebound, it is possible for variations in erosional efficiency to impact the exhumation history of a region.

In the absence of a reliable datum of known age and origin, I modeled a pre-incision maximum topography surface from which to measure the magnitude of incision (Appendix C). To create a pre-incision maximum topography surface model, the elevation of each cell within a DEM of the range was assigned the maximum value

within a 10-km radius of the target cell. The size of the sampling window was selected to be large enough to project a smooth surface across broad river valleys. The maximum topography surface was then smoothed using the mean from a moving window of 1 km radius to create a more realistic surface. The distribution of incision into the modeled maximum elevation surface was determined by subtracting the modern elevation from the modeled elevation on a per cell basis, thus showing the variation in geophysical relief throughout the range. For comparison between the NW-SJM and the S-SJM geophysical relief was sampled using the zones from Figure 7.

RESULTS

Apatite Thermochronology

Measured cooling ages in the San Juan Mountains illustrate that the region has not experienced uniform exhumation after early Miocene volcanism (Figure 9). In the NW-SJM, AHe ages from intrusions are between 2.8 ± 0.2 and 10 ± 0.6 Ma (Table 1) over an elevation range of 1300 m and are corroborated by AFT ages of 8.1 ± 5.8 to 14.6 ± 4.2 Ma (Table 2) over an elevation range of 1500 m. Exceptions are ages of 21.9 ± 1.5 and 20.1 ± 1.2 Ma from the Wilson Stock, a laccolithic intrusion in Cretaceous shales. In contrast, the S-SJM are characterized by AHe ages between 19.2 ± 1.2 and 31.9 ± 1.9 Ma over an elevation range of 800 m (Table 1). Cooling ages in the NW-SJM generally increase with elevation, whereas sample ages and elevations in the S-SJM show little relation (Figure 9B). Cooling ages reported are younger than published crystallization ages for the intrusions (Steven and Lipman, 1976; Bove et al., 2001). The presence of many hot springs in the San Juan Mountains

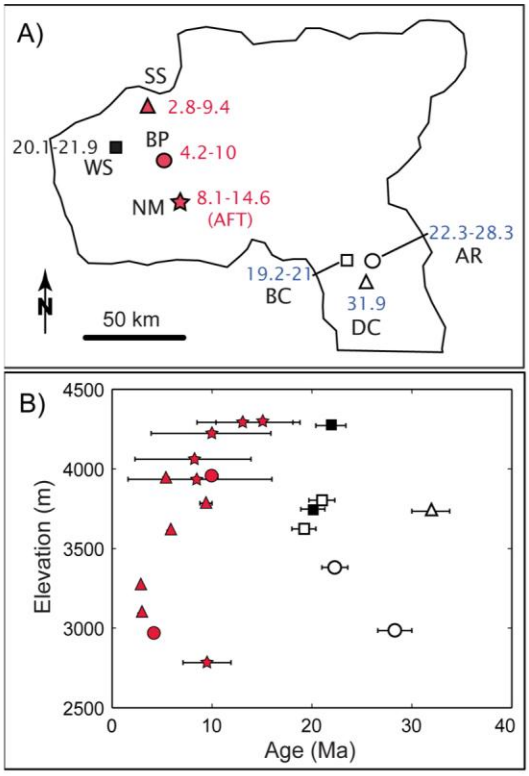

Figure 9. A) Map showing the sample sites for thermochronologic vertical transects with reference to the range front and swath profiles. B) Age/Elevation plot for all samples with analysis uncertainty indicated by error bars, where no error bars are evident the uncertainty falls within the width of the symbol. Symbols are consistent from A to B and include six AFT (Kelley, unpublished) ages 14 AHe ages.

Table 1. Summary table for Apatite (U-Th)/He dating. The data for each sample is the mean of three single grain aliquots unless indicated by an asterisk.

Sample	Elevation (m)	Latitude (ºN)	Longitude (ºW)	Age [Ma]	± [Ma]	stddev	U [ppm]	Th [ppm]	mass [µg]	Ft
Northwest										
NWSS1	3937	38.0134	107.793	5.4	0.3	0.7	6.8	19.6	10.7	0.79
NWSS2	3784	38.0115	107.792	9.4	0.6	1.9	6.9	24.7	1.8	0.63
NWSS3*	3604	38.0123	107.788	5.8	0.3	0.1	5.4	16.8	9.5	0.72
NWSS4	3262	38.0208	107.781	2.8	0.2	0.3	10.2	27.5	4.0	0.71
NWSS5	3084	38.0247	107.788	2.8	0.2	0.3	4.1	13.2	9.5	0.72
NWBP1	3954	37.7946	107.733	10.0	0.6	1.1	15.0	50.0	2.0	0.64
NWBP4*	2966	37.8165	107.729	4.2	0.3	0.9	13.5	48.6	4.3	0.68
NWWS1	4272	37.8604	107.994	21.9	1.5	0.8	5.8	28.6	1.0	0.57
NWWS4	3747	37.8493	107.944	20.1	1.2	1.6	17.4	39.8	3.2	0.68
South										
PBC1*	3803	37.3804	106.7	21.0	1.3	2.6	19.9	51.7	1.4	0.62
PBC2	3623	37.3808	106.695	19.2	1.2	0.1	24.0	33.9	2.1	0.62
PAR1	2985	37.3421	106.494	28.3	1.7	4.9	7.1	24.1	1.4	0.59
PAR3	3381	37.3805	106.547	22.3	1.3	3.6	10.4	22.2	9.1	0.72
PDC1*	3734	37.2821	106.588	31.9	1.9	0.8	3.4	15.2	2.8	0.68

* = One of three apatite grains in these smaples was likely contaminated by a zircon inclusion within the apatite crystal. Zircon typically has a much higher concentration of U and Th and thus the presence of a small amount within an apatite crystal can greatly affect the cooling age measured. As a result the anomalous age was not included in age or standard deviation calculation.

Table 2. Summary table for Apatite Fission Track dating from Dr. Kelley

Sample	Elevation (m)	Latitude (ºN)	Longitude (ºW)	Age [Ma]	Std. Error ± [Ma]
06NM01	4292	37.622	107.622	13.3	4.8
06NM02	4223	37.624	107.621	9.9	6
06NM03	4061	37.623	107.62	8.1	5.8
06NM04	3935	37.622	107.616	8.8	7.2
06NM05	4292	37.622	107.609	14.6	4.2
06NM06	2784	37.614	107.673	9.5	2.4

indicate above-normal heat flow, which could impact the results of low-temperature thermochronologic analysis. However, ground water geochemistry data indicate that the flow of hot ground water is controlled by fractures and that it rises rapidly from below reasonable depths for closure temperature thresholds for AHe and AFT systems (pers. comm. P. Morgan, 2008). Thus, our cooling ages are reflective of exhumation and not *in-situ* reheating at shallow depths.

Topographic and Climatic Characteristics

Comparison of modern precipitation and LGM ELA estimates from the NW-SJM and S-SJM show that the two areas are quite similar (Table 3). On average, the S-SJM receives about 10% more precipitation than the NW-SJM, although in both regions average annual precipitation is less than 100 cm reflecting the intracontinental setting of the range. LGM ELA is consistent with precipitation and lowest on the western flank of the S-SJM where annual precipitation is highest (Figures 5 and 6). The mean elevation for the two regions is different by only ~170 m (Table 3) with both areas averaging well over 3 km above sea level. In addition, the NW-SJM have greater average relief and maximum elevation relative to the S-SJM, however, the differences are not dramatic.

Table 3. Summary Table for topographic and climatic parameters for the northwestern and southern study regions.

	Elevation (m)			Relief (m)			Precipitation (cm/yr)			LGM ELA (m)		
Region	Max	Mean	stddev	Max	Mean	stddev	Max	Mean	stddev	Max	Mean	stddev
Northwest	3392	4332	376	869	1749	243	84	127	14.8	3475	3760	135
South	3224	4051	310	700	1336	199	93	127	15.2	3261	3502	117

Cirque Analysis

In the NW-SJM 69 northeast-facing cirques were identified compared with 16 in the S-SJM (Figure 10). The disparity in the number of cirques between the two study regions is likely a function of the width of the range and the dominant glacial form of the region. In the NW-SJM, cirque glaciers separated by ridges were quite prevalent, whereas the majority of the S-SJM was more akin to an ice cap-outlet glacier system centered just east of the Continental Divide. Cirque relief and average slope above cirque floors were

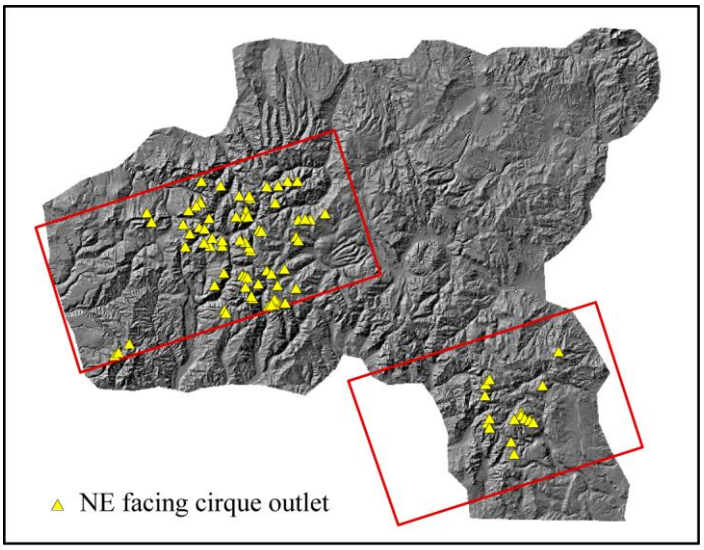

Figure 10. Map showing the location of northeast facing cirques within the limits of the swath profiles for the NW-SJM and S-SJM.

found to vary considerably between the two study regions (Figure 11). In the S-SJM mean cirque relief was 272 m ± 119 (all standard deviation calculations are 1σ unless otherwise noted) and the average slope of topography above cirque floors was 14.3° ± 10.5. In the NW-SJM, mean cirque relief was 419 m ± 124, and the average slope above cirque floors was 24.2° ± 12.2. For all northeast-facing cirques, bedrock lithology was not found to control the magnitude of relief (Figure 12).

Swath Profiles

Swath profile analysis indicates that the relationship between LGM ELA, average Quaternary ELA, and topography is different in the NW-SJM and S-SJM (Figure 13). In the northwest, modern precipitation, LGM ELA, modeled Quaternary average ELA, and mean topography follow a rising west-to-east gradient. Mean elevation and average Quaternary ELA show a significant relationship ($r^2 = 0.778$; p-value < 0.001), with mean elevation on average 309 m ± 153 below average Quaternary ELA. The relationship becomes stronger in the area where samples from vertical transects show young cooling ages intersect the northwestern swath. In a band extending 10 km to the east and west of the thermochronologic sampling sites (Figure 13), mean elevation and average quaternary

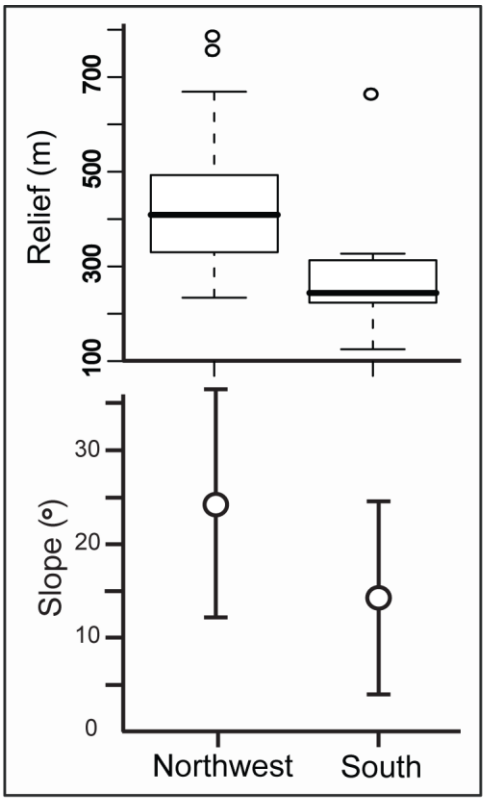

Figure 11. Graphs showing the range of cirque relief and slope above cirque floors for the NW-SJM and S-SJM. Cirque relief is displayed using box plots where the median is the heavy black line within the box. The slope graph shows the mean (circle) ± 1σ (tails) for all cells above the average Quaternary ELA for each zone.

controls. Average Quaternary ELA is closest to mean elevation at the range crest and moderately correlated with mean elevation (r^2 = 0.323; p-value < 0.001) across the limited distribution of cirques in the swath. The lack of cirques to the west of the southern ELA are strongly correlated (r^2 = 0.934; p-value < 0.001) and both measures of ELA become significantly closer to mean elevation with an average offset of 176 m (± 49, 1σ).

In the south, the variation between modern precipitation, glacial thresholds, and mean elevation shows no coherent pattern. Average Quaternary ELA shows little variation across the swath in contrast to modern precipitation and LGM ELA, reflecting a western source of moisture and orographic

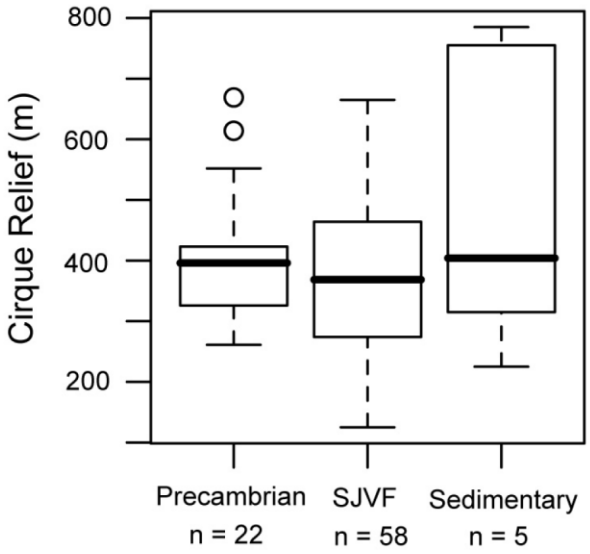

Figure 12. Comparative box plots showing the range of cirque relief values for all northeast facing cirques with respect to bedrock lithology (SJVF = San Juan Volcanic Field). The number of cirques within each sample is indicated below the rock type.

drainage divide and the inverse relationship between decreasing mean elevation and slightly increasing average Quaternary ELA that is evident east of the Continental Divide suggests a different relationship between climatic forces and topography in the S-SJM than in the NW-SJM.

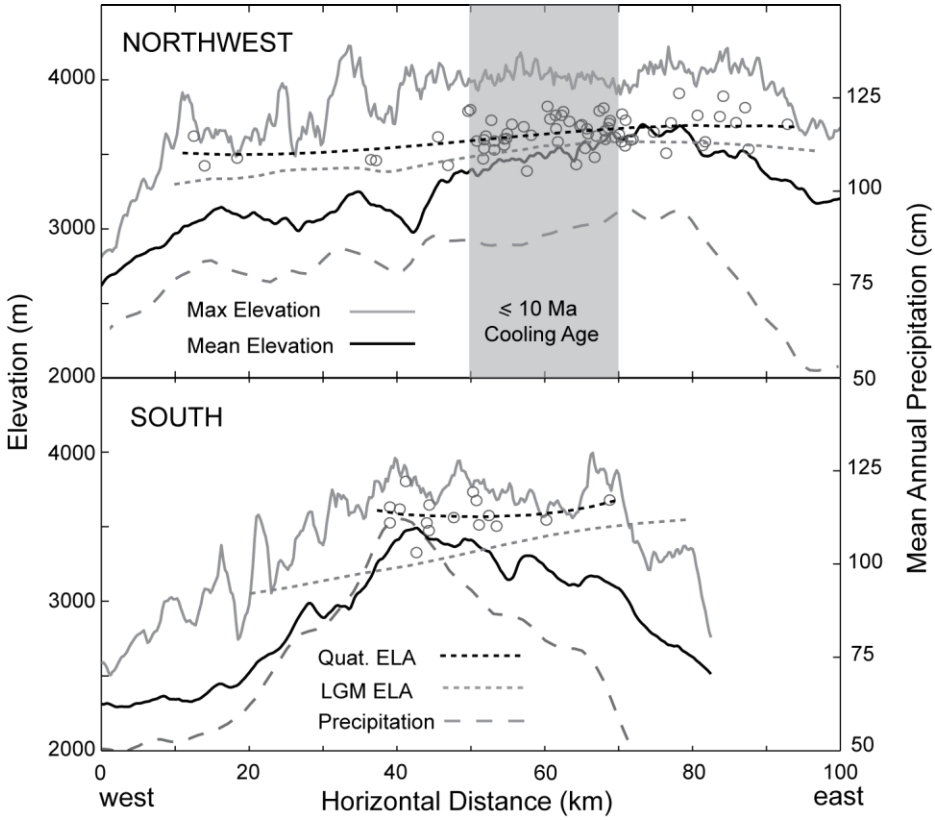

Figure 13. Topographic swath profiles for the northwestern and southern San Juans showing the relationship between climate and topography. Note how the correlation between mean elevation and average Quaternary ELA becomes stronger in the zone of young cooling ages in the northwestern swath (grey shaded region).

Erosion Models

The simple models of fluvial and hillslope erosive potential show differences between the NW-SJM and the S-SJM (Table 4). The average stream power of the NW-SJM is considerably higher and more variable than the S-SJM when sampled within each zone. It is likely this is due in part to the orientation of the large drainage area of the Animas River that runs parallel with the long axis of the NW-SJM sampling window,

Table 4. Summary Table for topographic and climatic parameters for the northwestern and southern study regions.

	Hillslope Model*			Stream Power Model (Ω X 10^9)			Geophysical Relief (m)		
Region	**Max**	**Mean**	**stddev**	**Max**	**Mean**	**stddev**	**Max**	**Mean**	**stddev**
Northwest	83.6	18.8	10.8	358.1	8	19.3	1802	660	338
South	83.2	16.9	10.9	51.6	3.9	4.5	1457	604	297

* = The units for the hillslope model are slope (°) times annual precipitation (cm/yr)

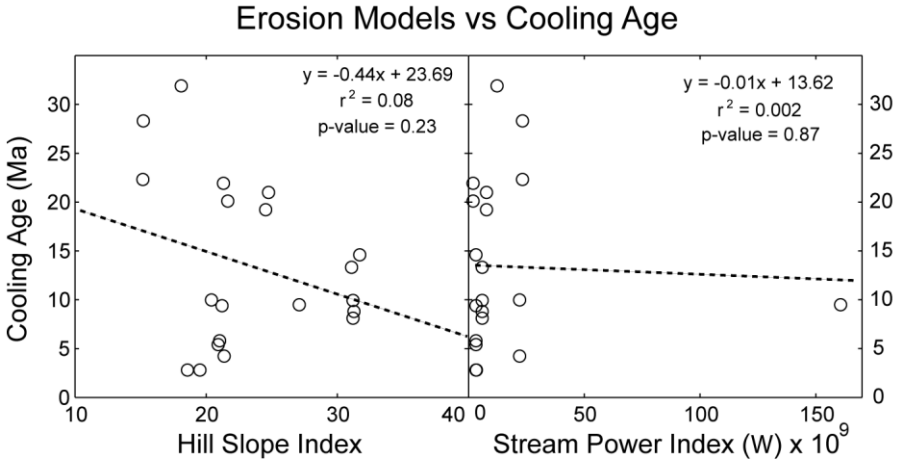

Figure 14. Cooling age plotted against the average hillslope index and the maximum stream power within a 5 km sampling window around each sample location.

which increases its signal in comparison to the large drainages of the S-SJM that are more perpendicular to the long axis of the sampling window. Average modeled hillslope erosion is quite similar for the two study areas and is reflective of their similarity in annual precipitation. When erosion potential was sampled around each thermochronologic sample site no linear relationship between exhumation age and the stream power ($r^2 = 0.002$, p-value = 0.87) or hillslope ($r^2 = 0.08$, p-value = 0.23) was found (Figure 14). The lack of correlation between cooling age and erosive potential suggests that although the NW-SJM do have high erosive potential, it does not appear to affect exhumation.

Incision and Isostatic Rebound

The modeled maximum topography surface reflects modern topography and is generally higher in the NW-SJM than the S-SJM (Figure 15A). When the modern topography is subtracted from the maximum topography surface, the greatest geophysical relief coincides with the deep river valleys draining the NW-SJM and the area with the lowest geophysical relief is the dry northeastern portion of the San Juan Mountains (Figure 15B). Incision is minimal along the Continental Divide and remains relatively low in the in the vicinity of cirques in both study regions. The average geophysical relief for the two regions is quite similar at 660 m ± 338 for the NW-SJM and 604 m ± 297 for the S-SJM. Because neither region shows a considerable difference in the distribution or magnitude of geophysical relief, it is likely that the isostatic response as a result of incision is likely to be nearly equal.

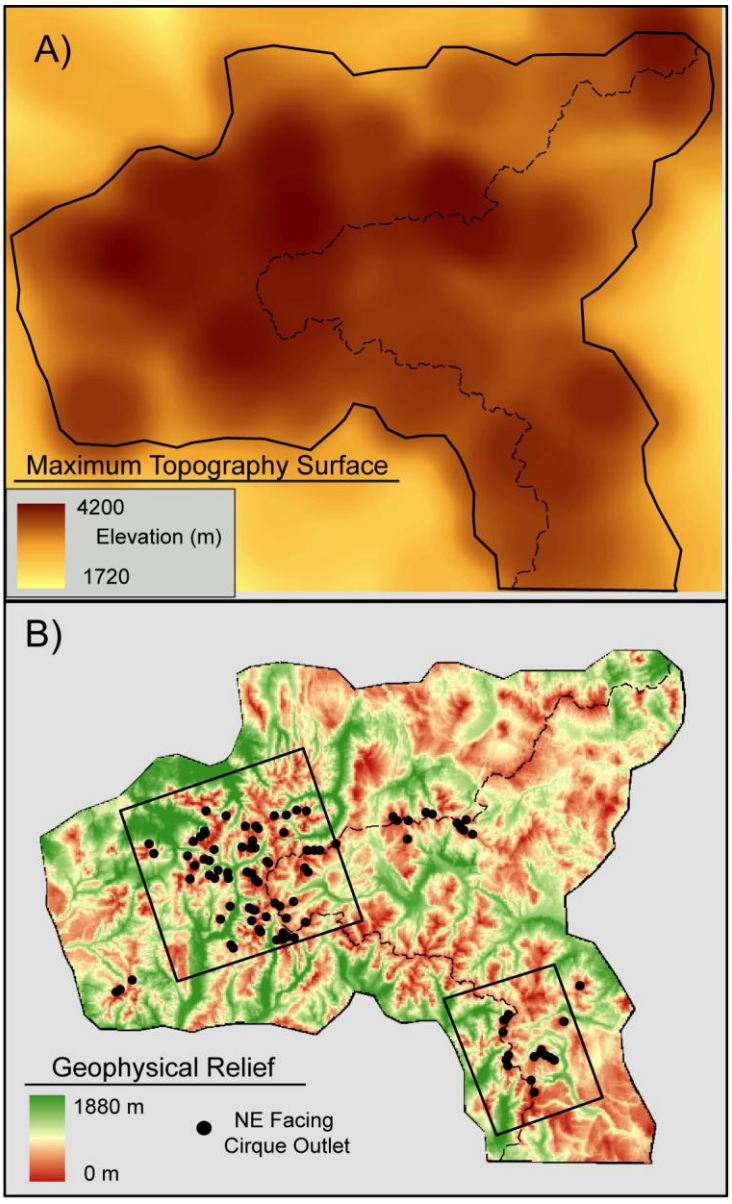

Figure 15. A) Map showing the elevation of the modeled maximum topography surface. B) Map showing the distribution of geophysical relief, the extent of modern incision into the modeled maximum elevation surface. The dashed line indicates the position of the Continental Divide.

DISCUSSION

From the results of the landscape analysis several similarities and differences between the NW-SJM and S-SJM are striking. Patterns of modern precipitation and LGM ELA indicate that both areas have experienced similar climate, which is further illustrated by the similarity of hillslope and fluvial erosive potential. The mean elevation and average geophysical relief of both regions are quite close, however, the cooling histories vary widely between the NW-SJM and S-SJM. Swath profiles show that maximum and mean elevation of the two regions show distinctly different relationships to both LGM and average Quaternary ELA and the morphology of northeast-facing cirques differs dramatically. These seemingly contradictory similarities and differences are instructive for understanding what is driving landscape evolution in the San Juan Mountains and how alpine glaciation has impacted this process during the Quaternary.

Driving Mechanism for Exhumation

Because erosion and exhumation are linked through the isostatic compensation of eroded material, it is possible that persistent differences in the rate of erosion between the NW-SJM and S-SJM could plausibly account for the different cooling histories of the two study regions. Table 4 shows that the mean and standard deviation of modeled hillslope erosion potential is nearly identical for the northwestern and southern regions and, therefore, unlikely to cause a difference in exhumation between regions. Average modeled stream power in the northwestern region is twice that of the southern region, which coincides with differences in maximum elevation. All but one of the 14,000 ft. peaks in the San Juan Mountains lie in the northwestern region (the other is in the central

San Juan Mountains along the Continental Divide) and when coupled with the higher stream power might suggest that greater erosion in the NW-SJM has led to higher maximum elevations. However, Table 3 shows that the mean elevation of the NW-SJM is higher than the S-SJM and the average geophysical relief of the two regions is nearly identical which makes the production of higher topography in the NW-SJM relative to the S-SJM through a decrease of mean elevation and an increase in geophysical relief unlikely. It is possible that the higher elevation of peaks in the northwestern region is inherited from the original topography of the volcanic field, however, the vertical transects of cooling ages from the northwest indicate a minimum of ~2 km of exhumation and erosion in the last 10 Ma, making the maintenance of inherited higher topography improbable. Finally, the focused analysis of the impact of stream power on cooling age (Figure 14) illustrates that although the northwest does have a higher average stream power, this difference does not have a noticeable affect on the cooling ages.

Given the lack of significant variability in erosive potential and the difficulty in explaining the current topographic high of the northwestern region through erosive processes, the simplest explanation for the variability of exhumation in the San Juans is through active tectonism. The lack of active faulting within the range suggests that epeiorgenic doming is the process that is driving exhumation and could be related to the Aspen anomaly, a region of low seismic velocities underlying central Colorado (Deuker et al., 2001). The Aspen anomaly is a tabular zone of low velocity material in the upper mantel that penetrates to considerable depth (> 200 km) and is comparable in size to the velocity anomaly associated with Yellowstone (Karlstrom et al., 2005), which coincides spatially with the highest and most rugged terrain in the Colorado Rockies (Figure 16)

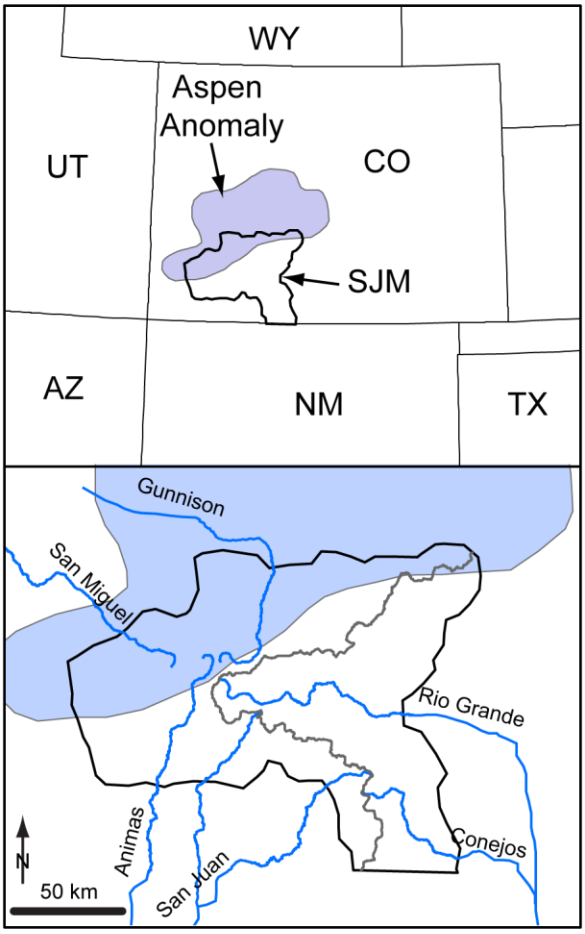

Figure 16. A) Map showing the location of the Aspen anomaly from Dueker et al. (2001) in central Colorado. B) Map showing the radial drainage pattern of the NW-SJM in relation to the mapped seismic anomaly. Note how the drainage pattern in the S-SJM is not radial and how the Continental Divide (grey line) is deflected to the east.

(Coblentz and van Wijk, 2007). The cause of the anomaly is currently being investigated (e.g. Karlstrom et al., 2007) and is beyond the scope of this discussion. The timing and magnitude of exhumation observed with AHe dating from this investigation in the NW-SJM is consistent with estimates of 2 km of exhumation during the late Cenozoic from the incision of the Colorado, Gunnison, and Arkansas Rivers (Coblentz and van Wijk, 2007). Active epeiorgenic uplift of the NW-SJM related to the Aspen anomaly could explain the more rugged character of the NW-SJM (Figure 1) and the radial drainage pattern of the area (Figure 16), which contrasts with the east and west directed drainages of the S-SJM. The difference in the drainage networks and the lack of young cooling ages in the S-SJM suggest that the two regions are not subject to the same tectonic controls. The cooling history of the S-SJM and the location of the highest and most rugged topography in the

NW-SJM suggest that the Rio Grande Rift has had little influence on late Cenozoic exhumation in the San Juan Mountains.

Landscape Evolution

During the Quaternary the character of glaciation was not consistent across the San Juan Mountains, with the NW-SJM dominated by cirque and valley glaciers and the S-SJM dominated by an ice cap-outlet glacier system centered just east of the Continental Divide. Climate and bedrock geology impact the erosive strength of glaciers (Hallet et al., 1996), however, in the San Juan Mountains neither accounts for the contrast in the cirque morphology or the relationship between glacial thresholds and topography for the two study regions. Average annual precipitation values are similar for both areas with little difference in the seasonality of precipitation or temperature. Bedrock geology differs between regions; however, the relief of cirques was not influenced by rock type (Figure 12). The Precambrian bedrock of the northwestern region should, if anything, have been more erosion resistant than the volcanic rocks and associated sediment of the south. Only the exhumation history of the two areas differs dramatically and suggests that the processes driving young rock uplift in the northwest have led to the generation of greater cirque relief and more pervasive glacial modification of the landscape.

Though stark differences exist in cirque morphology between the NW-SJM and the S-SJM, the distribution of geophysical relief across the San Juans reveals that the level of incision into the modeled maximum topography surface is quite similar for the two study regions. The mean geophysical relief for both regions was in excess of 600 m, which places the average valley well below the average Quaternary ELA. Most of the

large river valleys that drain the San Juan Mountains have been occupied by glacial ice, but the lack of glacially scoured lakes at the mountain front suggests that glacial erosion has done little to lower the base level of the fluvial system (Steven et al., 1995). This observation identifies the importance of the long-term dominance of fluvial erosion in the evolution of the San Juan Mountains. Quaternary glacial modification, though locally extensive, is mainly isolated high in the range where glacial erosion has ornamented the preexisting fluvial landscape.

The Glacial Buzzsaw in the San Juan Mountains

Despite the previous statement that glacial erosion has not been the dominant agent in landscape development in the San Juan Mountains, the mean relief of topography above cirque outlets in the NW-SJM is equal to that from the Cascade Range (Mitchell and Montgomery, 2006) and greater than that from the northern Basin and Range (Foster et al., 2008). In addition, the average slope of topography above cirque floors in the NW-SJM is 24° and steepens 27° in the area 10 km east and west of the axis of young cooling ages (Figure 13). These slopes are similar to the 29° average calculated for the Cascade Range. Mitchell and Montgomery (2006) used relief and slope above cirque floors to define an "envelope" above average Quaternary ELA where glacial and periglacial processes control summit elevation through enhanced erosion and creation and maintenance of threshold slopes. This envelope is the altitudinal range where the glacial buzzsaw exerts its strongest topographic control. The similarity of cirque morphology between the northwestern San Juans and other mountain ranges in western United States and the systematic increase of mean and maximum elevation with average Quaternary

ELA in the presence of active and spatially variable exhumation, suggests that glaciers exert a primary control on the elevation of the range.

To understand how glacial erosion has affected the evolution of the San Juan Mountains and to place the morphological changes in the context of previously studied mountain ranges, I propose a conceptual model to describe how topography transforms as a response to glacial erosion (Figure 17). First, a relative lowering of ELA; either through cooling climate or surface uplift, places preexisting fluvial topography above the ELA, the S-SJM are an example where no correlation between ELA and topography is evident and the range crest is centrally located.

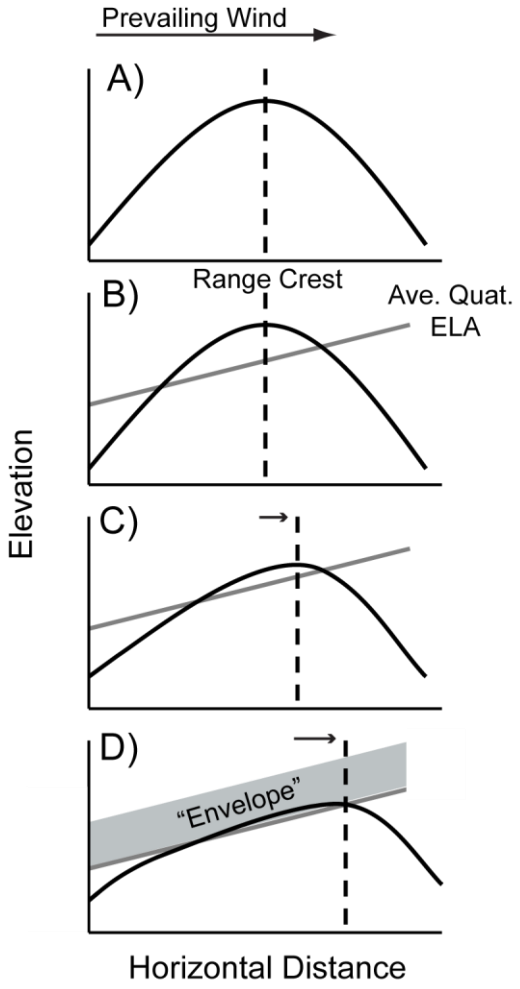

Figure 17. Conceptual model of topographic profiles that model the transformation of pre-glacial topography to topography controlled by the glacial buzzsaw. The solid black line is mean elevation, the solid grey line is average Quaternary ELA and the dashed black line shows the position of the range crest. A) Pre-glacial topography; B) Initiation of glaciation; C) Intermediate stage where mean elevation approaches the ELA and; D) Glacial buzzsaw model where max elevation (dashed grey line) is constrained within a topographic "envelope" (grey shaded area) and the range crest is deflected away from the prevailing wind.

Next, the conversion of fluvial topography through the creation of U-shaped valleys and cirques as a result of headward erosion lowers mean elevation by decreasing the amount of land area above the

ELA. The NW-SJM illustrate this stage where mean elevation adjusts to ELA and cirques approach common depth due to the limiting factors of threshold slopes and rock strength.

Finally, long-term glacial erosion produces a strong coupling between mean elevation and ELA, a control of summit elevation by excavating cirque basins where few peaks pierce the topographic "envelope", and a lateral offset of the range crest as a result of orographic effects on precipitation causing lower ELAs proximal to the moisture source. The topographic asymmetry that correlates with orographically controlled ELA has been observed in the Cascade Range, southeast Alaska, and the Himalaya (Mitchell and Montgomery, 2006; Meigs and Sauber, 2000; Brozovic et al., 1997 respectively).

The evolution of topography as described is not strictly time-dependent. In more dynamic settings with high precipitation and tectonic activity the transformation will occur quite fast and rates of exhumation and erosion may locally be quite high (e.g. Brozovic et al., 1997; Berger and Spotila, 2008). However, as the NW-SJM and the work of Foster et al. (2008) in the mountains of the Northern Basin and Range of Idaho and Montana indicate, areas with lower rates of tectonic uplift and lower precipitation rates can still produce a coupling between topography and climate thresholds.

The mountain ranges of the western United States exhibit considerable variation in their morphological response to Quaternary glaciation, yet maximum elevation and ELA systematically decrease with increasing latitude despite differences in tectonic setting, lithology, and climate. This relationship begs the question whether the elevation of the mountains is controlling the occurrence of glaciers or glaciers are controlling the elevation of mountains. The differing responses of the northwestern and southern San Juan Mountains appear to be a microcosm of this relationship, with the southern region

and its subdued topography and lack of evidence for active tectonism being just high enough to be glaciated and the rugged, tectonically active northwestern region where glaciers control elevation.

CONCLUSIONS

In the San Juan Mountains morphological differences between the northwestern and southern portions of the range coincide with differences in exhumation history derived from apatite (U-Th)/He and fission track dating. Climatically the two areas are quite similar and models of fluvial and hillslope erosion cannot explain the partitioning of old (>20 Ma) cooling ages in the southern region and young (<10 Ma) cooling ages in the northwestern region. Additionally, the northwestern region has greater maximum and mean elevation relative to the south, but the average geophysical relief is nearly identical between the two areas. These data suggest that erosion and isostatic rebound are an unlikely source for the variability of exhumation across the range. I propose that the northwestern portion of the range is experiencing epeirogenic uplift possibly related to uplift on the flanks of the Aspen anomaly, a large low velocity anomaly in the upper mantle that underlies the highest and most rugged topography in the Colorado Rockies (Dueker et al., 2001; Karlstrom et al., 2005; Coblentz and van Wijk, 2007).

The mean geophysical relief of valleys in the San Juan Mountains lies well below the average Quaternary ELA and it nearly equal in the northwest and south implying that Quaternary glaciation has done little to broadly affect the preexisting fluvial landscape. However, both relief and slope of topography above cirque floors were considerably greater in the NW-SJM relative to the S-SJM despite the similarity of climate, and suggest that active tectonic rock uplift in the NW-SJM led to greater glacial modification of the landscape. The S-SJM illustrate that glaciation alone does not dramatically modify preexisting topography and, as a result, shows little correlation between topography and

glacial thresholds. In contrast, the NW-SJM illustrate that small glaciers in less dynamic climatic settings are capable of keeping pace with slow uplift rates and as a result elevation can be limited based on climatically dictated glacial thresholds. The San Juans appear to be a microcosm for the diverse mountain ranges of the western United States, where tectonic activity and glaciation are variable, but elevation is broadly correlated with Quaternary glaciation thresholds. Climate, through glacial erosion, has limited the elevation of the San Juans and perhaps other mountains in the western United States and it appears the glacial buzzsaw is active, although manifest more locally to high topography, in a broad range of tectonic and climatic settings.

APPENDICES

APPENDIX A

ADDITIONAL DESCRIPTION FOR SELECTED TOPICS

DISCUSSED IN THE INTRODUCITON

Climate Change and Topography

Molnar and England (1990) noted that the global distribution of high mountain ranges and increased sedimentation rates during the late Cenozoic could not be attributed to a global tectonic event. Instead, to explain these observations they hypothesized that a positive feedback mechanism between erosion and isostatic rebound resulting from the global transition to icehouse climate conditions could produce both greater sedimentation rates and higher topography. They postulated that enhanced erosion (either through glacial processes or increased storminess) concentrated in valleys could remove material such that mean elevation would decrease while relief and summit elevations would increase as a result of isostatic compensation for the removed mass. Thus generating higher topography and increased sedimentation rates by increasing relief due to a change in the erosion regime resulting from a cooling climate. However, the correspondence between peak elevations and Quaternary glacial thresholds is striking (Broecker and Denton, 1990) with only a very small percentage of mountainous topography standing above the climatically dictated glacial threshold (Figure A1). These, perhaps conflicting observations helped trigger a large amount of research into the morphologic changes that mountains experience as a result of glacial erosion.

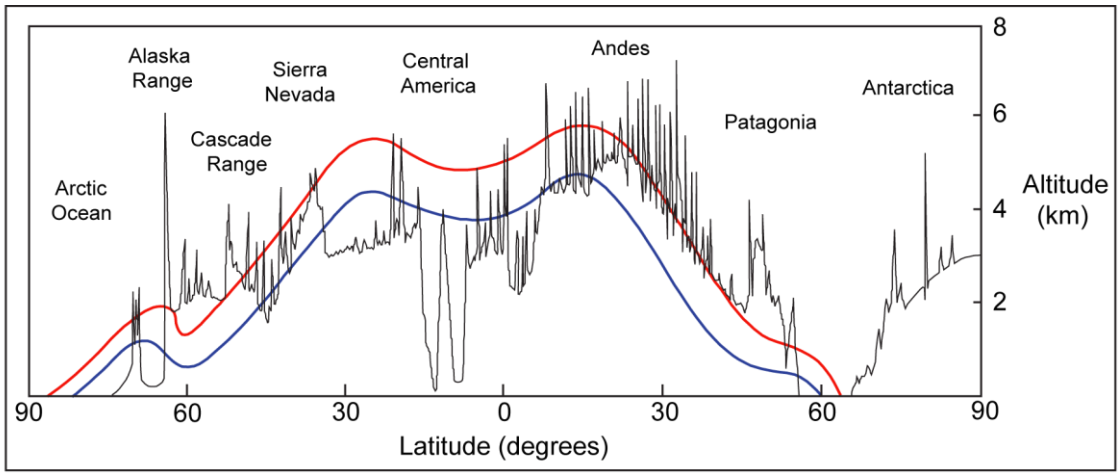

Figure A1. A topographic profile from north to south across the western margin of the North and South American continents showing the relationship between maximum topography and modern snowline (red line) and Last Glacial Maximum snowline (blue line). Adapted from Broecker and Denton (1990).

Fluvial vs. Glacial Erosion

For the cooling of global climate to profoundly change the distribution of topography within a mountain range, resulting in positive or negative altitudinal feedbacks, glacial erosion should be more effective than the fluvial or hillslope processes that preceded it. Recent studies have shown that glaciers erode bedrock over a wide range of rates (Hallet et al., 1996; Bishop et al., 2002). However, Hicks et al. (1990) found that fluvial sedimentation rates can equal those of small glaciated basins in the Southern Alps of New Zealand implying that glacial erosion is no more effective than fluvial. Koppes and Hallet (2002) acknowledged the difficulty of accurately measuring the rate of sediment production in glaciated landscapes due to the complex interactions of many variables that influence the erosive power of a glacier. As a result the debate is ongoing as to the relative effectiveness of glacial versus fluvial erosion at short time scales (e.g. Harbor and Warburton, 1993).

For the onset of alpine glaciation to lead to a positive or negative feedback associated with maximum topographic extent and isostatic rebound, glaciers would need to sufficiently alter the distribution and magnitude of relief from previously fluvial landscapes. In Laramide uplifts of the Rocky Mountains, Small and Anderson (1998) found that differential erosion between glaciated valleys and "summit flats" increased the "geophysical relief" or missing mass in the mountain range through the relief generated by incision into a once planar surface. Comparative studies based on the relief and volume of adjacent glaciated and nonglaciated valleys in the Olympic Mountains of Washington, (Montgomery, 2002) and central Idaho (Amerson et al., 2007) imply that glacial erosion is more efficient at removing mass over longer times scales than fluvial processes. In the Sierra Nevada of California, glaciers were found to flatten valley profiles unlike rivers; however, increases in relief were relatively minor and largely a result of the headward erosion of cirques (Brocklehurst and Whipple, 2002). It was also found in the Sierra Nevada and central Idaho that relief in both fluvial and glacial valleys was proportionate to drainage area. Studies in the Kyrgyz Range and the Bitterroots of Montana (Oskin and Burbank, 2005; Naylor and Gabet, 2007 respectively) confirmed the tendency of glaciers to erode laterally at two to four times the rate that they incise valley floors, perhaps indicating that relief generation is minor part of the transition from a non-glacial to glacierized landscape.

The Equilibrium Line Altitude (ELA)

The ELA is means of measuring the threshold of glaciation and is a climatically sensitive line separating the up-valley zone of accumulation (positive annual mass

balance) from the down-valley zone of ablation (negative annual mass balance) and adjusts to changes in precipitation and temperature. The complexity of the ELA for a region is largely dependent on the scale of observation (Humlum, 1986) and the term is used to discuss climatic variations on anything from an individual glacier to the entire western United States. A cooling of climate, an increase of precipitation, or some combination of the two lowers the ELA of a glacier allowing it to extend further down valley. Similarly, if climate remains the same and the land surface rises through either tectonic or isostatic uplift more, land area will be forced into the zone of accumulation. An increase in accumulation leads to an increase in mass flux within the glacier that results in higher ice sliding velocities and greater erosion rates that are concentrated at or near the ELA (Andrews, 1972; Hallet et al., 1996; Tomkin and Braun, 2002).

The Glacial Buzzsaw

The term "glacial buzzsaw" was coined to describe the relationship between mean elevation and ELA in the northwestern Himalaya surrounding Nanga Parbat (Brozovic et al., 1997). Despite large variations in physiography, lithology, and rock uplift rate, including some of the highest measured rock uplift rates in the world, eight study regions were shown to have similar hypsometry (frequency distribution of elevation within the study region) with a peak in frequency tightly constrained by the regional ELA and only a small fraction of land area extending above the climatic barrier. This relationship led Brozovic et al. (1997) to conclude that glaciers in the Nanga Parbat area were capable of eroding at rates equal to those of tectonic rock uplift and as such could control the altitude achieved by the actively deforming orogen. Subsequent studies in southern

Alaska (Meigs and Sauber, 2000; Spotila et al., 2004), the Andes (Montgomery et al. 2001; Thomson, 2002), the Cascade Range of Washington state (Mitchell and Montgomery, 2006), and the Northern Basin and Range of Idaho and Montana (Foster, et al., 2008) have demonstrated that the correlation between glacial thresholds and the average height of actively deforming mountain ranges is not isolated to the Himalaya.

Though some of the areas where the relationship between topography and ELA has been described as a glacial buzzsaw are experiencing rapid (>1 mm/yr) tectonic rock uplift rates, others such as the Northern Basin and Range are not and therefore rapid exhumation rates are not a requirement of the process. The following is a description of how glacial erosion transforms the hypsometry (area altitude distribution) of a mountain range and imposes a control the elevation of the range based on the climatically dictated ELA.

The flat floors of cirques, formed at the Quaternary average position of the ELA (Porter, 1989), are created at the expense of fluvial hillslopes and concentrate land area near the ELA (Figure A2). Ridges separating different drainages are narrowed, pushing them towards threshold steepness, where rock strength becomes an important constraint on the relief that is supported above the valley floor. Peaks can protrude well above the ELA (the summit of Nanga Parbat standing more than 8 km above sea level is an example this from the Himalayan study) however the hypsometric effect of isolated high topography is negligible. As a result of these erosive patterns and resultant feedbacks, Mitchell and Montgomery (2006) described how topography in the Cascades occupied an "envelope" ~ 600 m above the Quaternary average ELA, effectively describing how glacial erosion can control the elevation of summits and ridges through persistent erosion

in adjacent valleys. Simply put, the glacial buzzsaw model describes how climate dictates the average position of ELA in an area, the ELA determines the elevation of cirques, the increase of land area at the altitude of cirques sets the mean elevation, isostatic rebound responds to changes in the mean elevation, and relief and topographic extent are controlled by the creation and maintenance of threshold slopes.

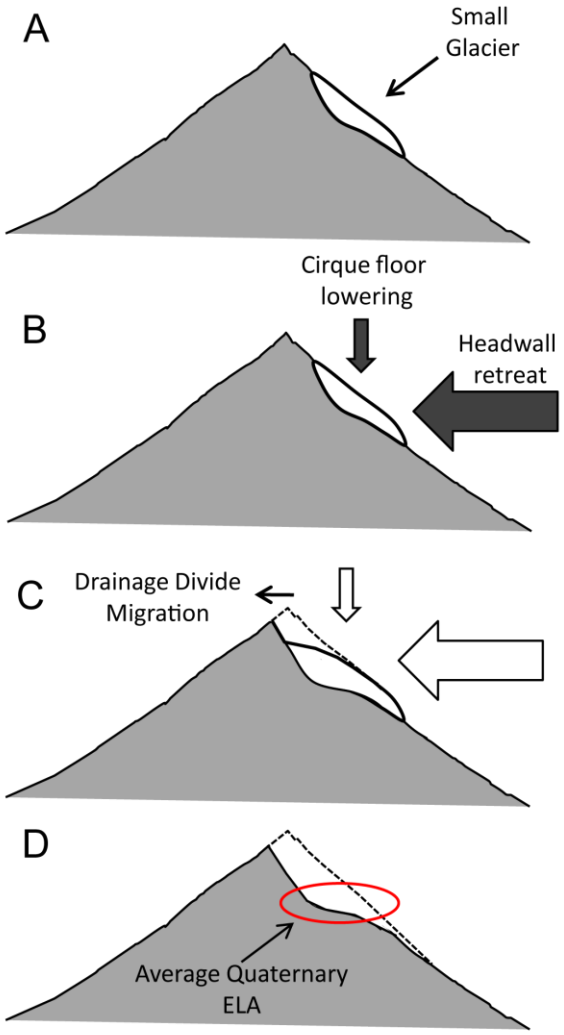

Figure A2. Conceptual model showing how alpine glaciation affects the hypsometry of mountains. A) A small glacier grows on preexisting topography. B) Glacial erosion results in 2-3 times more erosion of the headwall than the cirque floor (see text for references). C) The result of progressive headwall erosion is a migration of the drainage divide. D) When the glacier melts, a steep headwall and a flat cirque floor have replaced the lower angle topography that preceeded it, which concentrates more land area at the elevation of the cirque floor and represents the average Quaternary ELA.

APPENDIX B

ADDITIONAL DESCRIPTION OF STUDY AREA

The San Juan Peneplain

The modern Continental Divide snakes through the radial drainage pattern of the range and separates the more deeply dissected western portion from the more subdued and plateau-like eastern portion, however, following the close of major volcanism ca. 26 Ma, little is known of the physiographic evolution of the San Juan region. Atwood and Mather (1932) described an expansive peneplain surface that was cut into a high plateau of volcanic material fitting the classic Davisian model for landscape evolution (Figure A3) . Through numerous outcrops of accordant ridgelines and flat expanses they were able to compose a contour map of the erosion surface throughout the San Juan region that ranged in elevation from 2,350 to 4,150 m and was studded with monadnocks protruding above the mature landscape. The wide range in elevation for the outcrops of the San Juan peneplain was explained by regional doming of the erosion surface before all residual hills and peaks could be reduced to base level. Steven (1968) revisited the peneplain concept and determined that geological relations between many of the supposed remnants of the surface did not support an erosional origin. Using improved understanding of the geomorphic and volcanic history of the region Steven described the many outcrops of suspiciously flat ground as constructional features related to evolution of the volcanic field and assigns no specific process to their creation. Instead of widespread peneplanation as envisioned by Atwood and Mather, Steven suggests that the post-volcanic landscape of the San Juans remained largely unaltered until late Cenozoic regional doming led to fluvial incision and the creation of the rugged modern topography.

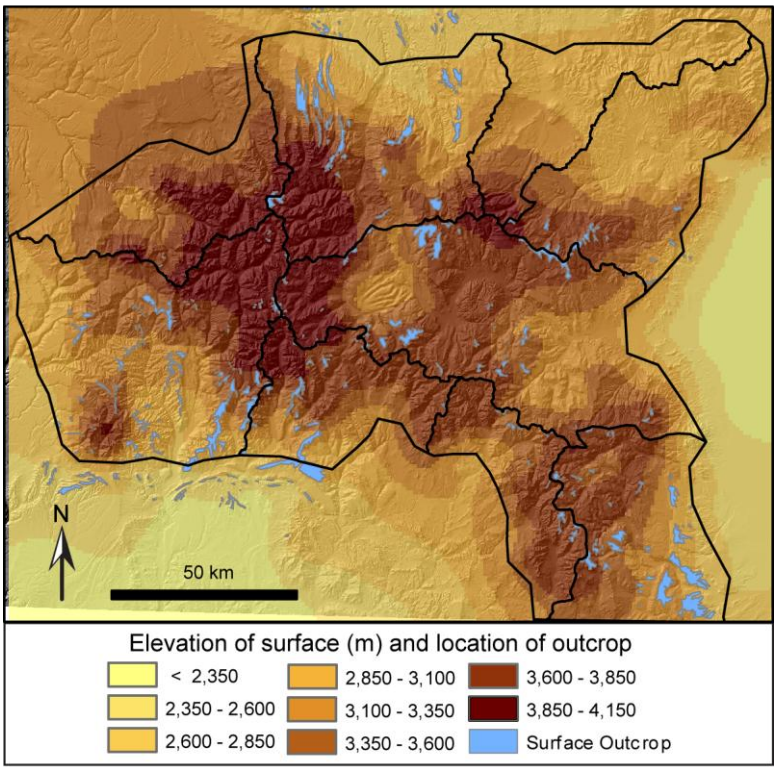

Figure A3. Map showing the modern elevation of the San Juan peneplain as mapped by Atwood and Mather (1932). Blue polygons show the location of outcrops used by Atwood and Mather (1932) to map the peneplain surface.

SNOTEL Precipitation Data

Precipitation data from 18 SNOTEL stations in the San Juan Mountains was collected to assess the spatial variation of the seasonality of precipitation across the range. The SNOTEL stations operated by the NRCS are located along the Continental Divide and concentrated in the northwestern portion of the range (Figure A4). Table A1 gives the monthly and annual average precipitation for all 18 SNOTEL sites over a period from 1971 to 2000 and was obtained from through the NRCS web site (http://users.frii.com/global-cgi-bin/cgiwrap/cpacheco/work/prec/avg_inc_summary?st

_fips=08 accessed on 7/7/08). The seasonality of precipitation was calculated through the following process and is displayed in Table A2: First, the mean annual precipitation for each site was divided by 12 to produce a monthly mean precipitation value. Second, the actual monthly mean precipitation value from Table A1 was divided by the calculated monthly mean for all 12 months at all 18 stations producing ratios where values greater than one indicate that more precipitation falls during that month than the monthly mean value calculated from the annual total, a value less than one indicates the opposite relationship. Finally, the ratios for all 18 stations were average for month to illustrate the seasonal variation of precipitation in the San Juan Mountains, which is graphically illustrated in Figure A5 using boxplots. The monthly boxplots indicate that winter through early summer are the wettest months in the San Juan Mountains and that fall is the driest time of the year. The short tails on the boxplots of Figure 5 indicate that the variation of the seasonality of precipitation in the San Juan Mountains is relatively minor between the 18 stations.

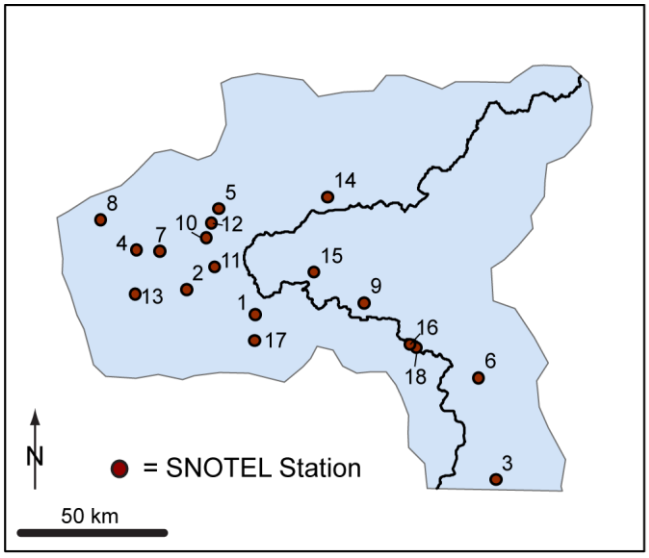

Figure A4. Map showing the location of the 18 SNOTEL weather stations used to analyze annual precipitation pattern the in the San Juan Mountains. Numbers correspond to the Site ID on Table A1.

Table A1. Monthly average precipitation for 18 SNOTEL locations in the San Juan Mountains

SNOTEL Site	ID #	Jan.	Feb.	Mar.	April	May	June	July	Aug.	Sept.	Oct.	Nov.	Dec.	Annual Mean (in.)
Beartown	1	4.2	4.5	4	3.7	3.5	3.7	3.5	3	1.8	2.6	3.4	3.7	41.6
Cascade	2	3.1	3.4	3.3	3.3	3.4	3.6	3	2.1	1.3	2.4	3.1	3	35
Cumbres Trestle	3	3.3	4.1	4	4.5	5	4.8	3.2	2	1.2	2.1	3	2.5	39.7
El Diente Peak	4	2.9	3	3	3.4	3.6	4	3.6	3.2	1.5	2.2	2.6	2.2	35.2
Idarado	5	2.8	3.2	3	2.8	2.8	3.4	3.3	2.4	1.4	2	2.5	2.4	32
Lily Pond	6	2.9	3.6	3.6	3	3.7	3.7	3.2	1.9	1.1	2.3	2.7	2.1	33.8
Lizard Head Pass	7	2.8	2.7	2.6	2.8	2.9	3.3	3	2.8	1.3	2.7	3.1	2.5	32.5
Lone Cone	8	2.9	3.3	3.2	3.6	3.7	4	3.3	2.6	1.4	2.5	2.7	2.6	35.8
Middle Creek	9	4.3	4.2	3.5	3.2	4.1	4.5	3.8	2.6	1.6	2.7	3.3	3.7	41.5
Mineral Creek	10	2.9	2.9	2.7	2.8	3	3.4	3	2.5	1.3	2.3	3.1	2.8	32.7
Molas Lake	11	3.1	3.1	3.7	3.3	3.7	3.4	3.4	2.5	1.4	2.3	3	2.9	35.8
Red Mountain Pass	12	3.8	4.2	4.1	4.1	4.2	4.5	4.4	2.9	1.6	2.5	3.2	3	42.5
Scotch Creek	13	2.6	2.7	2.4	3.1	3.5	4.3	3	2.1	1.1	2	2.5	2.1	31.4
Slumgullion	14	2.5	2.4	1.9	1.8	1.9	2.3	2.7	1.9	1.1	2.1	2.4	2	25
Upper Rio Grande	15	2.5	2	1.4	1.4	1.7	2.2	2.2	1.5	1.1	1.9	2.5	2.3	22.7
Upper San Juan	16	4.8	5.5	5.3	5.5	5.6	6	4.4	2.9	1.6	2.9	3.7	3.9	52.1
Vallecito	17	3.1	3.3	3.4	3	3.5	3.9	3.3	2.3	1.4	2.7	3.7	3.2	36.8
Wolf Creek Summit	18	4.8	5.6	5.2	5.5	6.1	6.4	4.8	3.1	1.6	2.7	3.5	3.7	53

Table A2. Table showing the seasonality of precipitation for the 18 SNOTEL stations in the San Juan Mountains

SNOTEL Site	Monthly Mean (in.)	Ratio of Monthly Mean Calculated for Each Month											
		Jan.	Feb.	Mar.	April	May	June	July	Aug.	Sept.	Oct.	Nov.	Dec.
Beartown	3.47	1.21	1.30	1.15	1.07	1.01	1.07	1.01	0.87	0.52	0.75	0.98	1.07
Cascade	2.92	1.06	1.17	1.13	1.13	1.17	1.23	1.03	0.72	0.45	0.82	1.06	1.03
Cumbres Trestle	3.31	0.09	1.24	1.21	1.36	1.51	1.45	0.97	0.60	0.36	0.63	0.91	0.76
El Diente Peak	2.93	0.99	1.02	1.02	1.16	1.23	1.36	1.23	1.09	0.51	0.75	0.89	0.75
Idarado	2.67	1.05	1.20	1.13	1.05	1.05	1.28	1.24	0.90	0.53	0.75	0.94	0.90
Lily Pond	2.82	1.03	1.28	1.28	1.07	1.31	1.31	1.14	0.67	0.39	0.82	0.96	0.75
Lizard Head Pass	2.71	1.03	1.00	0.96	1.03	1.07	1.22	1.11	1.03	0.48	1.00	1.14	0.92
Lone Cone	2.98	0.97	1.11	1.07	1.21	1.24	1.34	1.11	0.87	0.47	0.84	0.91	0.87
Middle Creek	3.46	1.24	1.21	1.01	0.93	1.19	1.30	1.10	0.75	0.46	0.78	0.95	1.07
Mineral Creek	2.73	1.06	1.06	0.99	1.03	1.10	1.25	1.10	0.92	0.48	0.84	1.14	1.03
Molas Lake	2.98	1.04	1.04	1.24	1.11	1.24	1.14	1.14	0.84	0.47	0.77	1.01	0.97
Red Mountain Pass	3.54	1.07	1.19	1.16	1.16	1.19	1.27	1.24	0.82	0.45	0.71	0.90	0.85
Scotch Creek	2.62	0.99	1.03	0.92	1.18	1.34	1.64	1.15	0.80	0.42	0.76	0.96	0.80
Slumgullion	2.08	1.20	1.15	0.91	0.86	0.91	1.10	1.30	0.91	0.53	1.01	1.15	0.96
Upper Rio Grande	1.89	1.32	1.06	0.74	0.74	0.90	1.16	1.16	0.79	0.58	1.00	1.32	1.22
Upper San Juan	4.34	1.11	1.27	1.22	1.27	1.29	1.38	1.01	0.67	0.37	0.67	0.85	0.90
Vallecito	3.07	1.01	1.08	1.11	0.98	1.14	1.27	1.08	0.75	0.46	0.88	1.21	1.04
Wolf Creek Summit	4.42	1.09	1.27	1.18	1.25	1.38	1.45	1.09	0.70	0.36	0.61	0.79	0.84
Mean fraction of monthly mean		*1.03*	*1.15*	*1.08*	*1.09*	*1.18*	*1.29*	*1.12*	*0.82*	*0.46*	*0.80*	*1.00*	*0.93*
Standard Deviation		*0.25*	*0.10*	*0.14*	*0.15*	*0.16*	*0.14*	*0.09*	*0.13*	*0.06*	*0.12*	*0.14*	*0.13*

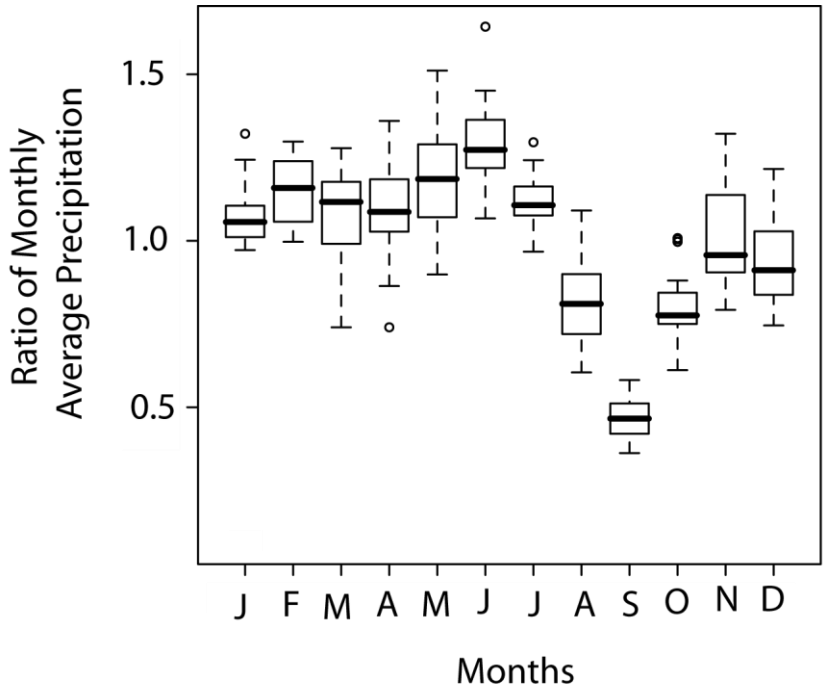

Figure A5. Comparative box plots showing the cumulative monthly variation in precipitation for all 18 SNOTEL weather stations in the San Juan Mountains. Please see the description in the text for the how this summary figure was created.

APPENDIX C

ADDITIONAL DESCRIPTION OF METHODS

Apatite Thermochronology

Thermochronology is a form of radiometric dating where the retention of the daughter products from the spontaneous decay of unstable parent isotopes is thermally dependent. Differences in the chemical composition and crystal structure of minerals that concentrate radiogenic isotopes result in different diffusion characteristics of the daughter products and as a result different minerals have unique closure temperatures. In apatite thermochronology, the spontaneous decay of ^{238}U and ^{232}Th (and to a much lesser degree ^{235}U and ^{147}Sm) produces ^{4}He alpha particles that diffuse quickly out of the crystal grain above ~70 °C (Farley, 2000). It is important to note that the closure temperature of apatite is not a discrete boundary, but rather it is defined by a partial retention zone between 40-80 °C where all ^{4}He is neither entirely retained nor lost and is similar to the partial annealing zone of fission track thermochronologic systems (Stockli et al., 2000). The depth of the closure temperature within the crust is dependent on the local geothermal gradient, the rate that material is moving through the system, and topographic perturbations to the shallow geotherms, however, in most crustal settings the closure temperature for apatite (U-Th)/He ages is at 2-3 km depth (Ehlers and Farley, 2003). Once an apatite grain has cooled below the closure temperature, ^{4}He accumulates within crystal lattice as a result of the continued decay of the unstable isotopes, which effectively starts the clock on the thermochronologic age of the apatite grain. The clock continues run until the grain is reheated above the closure temperature that causes the ^{4}He to diffuse out of the system. This reheating is hopefully carried out under high vacuum in a lab equipped to analyze the gas, however, it can also be caused by other processes

several of which are important to consider for this study. Potential causes shallow reheating are contact metamorphism through hydrothermal or magmatic processes, excessive burial, and surface exposure to forest fire and lighting has also been shown to affect cooling ages (e.g. Mitchell and Reiners, 2003), which were considered when selecting the sampling locations.

Sample Preparation and Selection

Apatite, which is a common accessory mineral in igneous rocks, was separated from the whole-rock samples using a series density and magnetic sorting techniques. Once the apatite was isolated, individual grains were selected for helium extraction based on the purity, size, and quality of the grains using an optical microscope. Mineral purity was important because inclusions of different minerals were common in the apatite of the San Juan Mountains. Inclusions are problematic for cooling age calculations because different minerals concentrate radiogenic isotopes in different abundances, for example a very small inclusion of zircon, which has a higher concentration of U and Th would make the age calculation older than a normal apatite because of the greater contribution of helium. Grain size is important because when spontaneous decay of a radiogenic atom occurs, the helium particles are shot out 20 microns from the decay site. If the decay site is within 20 microns of the rim of the grain, then it is possible that the helium could be ejected from the grain and not retained even if the grain was below the closure temperature. To correct for the loss of helium through the ejection of particles, the volume to surface area ratio of the grain is used to predict the probable amount of loss given a homogenous distribution of radiogenic isotopes within the grain. Below a grain

size of ~70 microns the correction (known as the FT correction on Table A4) becomes large enough that the uncertainty of the age calculation precludes dating the grain. Finally, any defect in the crystal structure of the grain can act as a conduit for helium to escape and therefore intact euhedral grains are the most desirable (refer to Farley, 2002 for detailed review of selection criteria and analytic techniques).

Helium extraction and U-Th-Sm concentration was carried out at the (U-Th)/He Laboratory at Kansas University which is run by Dr. Daniel Stockli. Due to the variable quality of the apatite from the San Juan Mountains, three single-grain aliquots were tested from each datable sample. Each aliquot was packaged in a platinum tube and heated using a Nd-YAG laser to release the helium from the grain. The ^{4}He that was released from each sample was then spiked with a known amount of ^{3}He, the ratio of the two was then analyzed using a Blazers Prisma QMS-200 quadrupole mass spectrometer to derive the ^{4}He content. The platinum tubes containing each aliquot were then recovered and analyzed for their U, Th, and Sm concentration using a Fisons/VG PlasmaQuad II Inductively Coupled Plasma Mass Spectrometer (ICP-MS). The data for all aliquots of each sample can be found on Table A4.

Topographic and Climatic Characteristics

This grid-based analysis focusing on the NW-SJM and S-SJM was conducted using 1 km gird cells of various datasets sampled over the entire area of each study zone. The rationale for the coarse nature of 1 km grid cell sampling was two-fold: First, the resolution of data layers is not universal; elevation data from Digital Elevation Models (DEMs) is commonly available at a 30 m gird cell scale that is proportionally to a USGS

1:24,000 topographic quad, whereas precipitation data used for this study was generated using point measurments of annual precipitation (the density of these measurements is dependent on location) in conjunction with an orographic precipitation model to produce an estimate of annual precipitation across a wide area. It would be irresponsible to imply that the precipitation estimate was accurate to the same scale as the elevation data and therefore one must use a coarser scale when analyzing the two. The second reason for using a coarse 1 km scale was computational, the San Juans cover a broad area and encompass over 20,000 km^2 within the nine study zones, a finer scale of analysis would increase this number dramatically, making data management and analysis more cumbersome without meaningfully impacting the output.

Elevation was sampled using a 30 m DEM from the National Elevation Dataset from the USGS that was resampled to 1 km resolution. For all Resampling to a 1 km grid cell is accomplished by taking the mean of all of the 30 m grid cells within the 1 km cell, thus resampling does result in a smoothing of topography. Relief was calculated by finding the difference between the maximum and minimum elevation within a sampling window of 2 km radius for each cell using the original 30 m DEM. The size of the sampling window was chosen to be large enough to capture the area of an average cirque or hillslope, but small enough so as not to sample topography from different ridgelines across larger valleys. Annual precipitation data from the PRISM Group was converted to a 1 km grid format with metric units from a shapefile with precipitation magnitudes in inches. Elevation, relief, and annual precipitation values were sampled from each cell within the nine sampling zones. Glaciation for each study zone was calculated by finding

the percent of land area within each zone that was covered in ice during LGM conditions as mapped by Atwood and Mather (1932).

LGM ELA Data

Table A3. LMG ELA estimations for 77 glaciers in the San Juan Mountains, used by permission from Eric Leonard.

Name	Side of Continental Divide	LGM ELA Estimate (m)	UTM Northing	UTM Easting (Zone 13N)
CHAMA	W	3170	4104000	361000
CONEJOS	E	3338	4113000	373000
NAVAJO	W	3200	4114000	351000
BLANCO	W	3018	4121000	343000
S.S.CREEK	W	3231	4129000	341000
SAND CK	W	3018	4133000	340000
ALAMOSA	E	3505	4139000	373000
SAN JUAN	W	3170	4142000	346000
LP 1	W	3231	4143000	224000
LP 4	W	3292	4143000	229000
4 MILE	W	2957	4144000	320000
TURKEY	W	3018	4145000	324000
WEST FORK	W	3231	4147000	332000
LP 2	W	3109	4148000	224000
PINOS	E	3353	4150000	362000
LP 5	W	3292	4151000	233000
PIEDRA	W	3277	4152000	316000
LP 3	W	3200	4153000	229000
GRAHAM PK	W	3231	4153000	294000
FLORIDA	W	3414	4154000	266000
PINOS	W	3475	4155000	285000
MIDDLE	W	3353	4156000	312000
HUERTO	W	2987	4158000	307000
VAL	W	3581	4159000	278000
WEMIN	W	3109	4159000	299000
SOUTH FK	E	3277	4160000	348000
FISCHER	E	3523	4169000	334000
FISH MT W	E	3200	4171000	328000
FISH MT E	E	3338	4171000	330000
RICO SW	W	3292	4172000	237000
RICO S	W	3322	4172000	238000

Table A3 Continued

ANIMAS	W	3475	4172000	257000
FISH MT N	E	3307	4172000	329000
RICO W	W	3200	4174000	235000
RICO NW	W	3115	4176000	235000
EAGLE PK	W	3353	4178000	230000
RICO N	W	3284	4178000	236000
MAIN IS	E	3399	4181000	295000
W GRIZ PK	W	3536	4182000	245000
WILSON 1	W	3383	4189000	234000
DOLORES	W	3292	4189000	246000
WILSON 2	W	3581	4191000	234000
WILSON 5	W	3484	4191000	238000
LIZ HEAD	W	3490	4192000	242000
WILSON 3	W	3627	4193000	234000
TINY	E	3597	4195000	296000
PROSP W	W	3444	4197000	249000
HALFMOON	E	3719	4197000	340000
PROSP E	W	3475	4198000	251000
WILSON 4	W	3139	4199000	236000
SM-BILK	W	3117	4199000	248000
MINERS	E	3566	4199000	322000
MESA PK	E	3536	4199000	357000
CREEDE W	E	3536	4200000	328000
CREEDE E	E	3612	4200000	334000
LA GARITA	E	3658	4200000	343000
PLAT SW	W	3505	4202000	312000
PLAT TINY	E	3749	4202000	315000
ST.CR-HEN	E	3758	4204000	290000
PLAT NW	W	3505	4204000	313000
ORGAN MT	E	3597	4204000	337000
CAMPBELL	W	3155	4206000	250000
ROUGH	W	3475	4207000	316000
MINERAL	W	3536	4207000	321000
SPRING	W	3536	4208000	326000
WHIP-RAF	W	3277	4209000	246000
RAT	E	3627	4209000	326000
HAYDEN PK	W	3353	4212000	243000
WTHSE W	W	3261	4213000	258000
WTHSE E	W	3322	4213000	259000
DALLAS	W	3139	4214000	248000
SNEFFELS	W	3322	4214000	254000
UNCOMPAGHRE	W	3292	4214000	264000
WILDHORSE	W	3475	4216000	273000
CANNIBAL	W	3505	4225000	311000
B CIMMERON	W	3033	4233000	278000
BLUE	W	3292	4233000	292000
L CIMMERON	W	3109	4239000	285000

Surface Modeling

The erosion surface mapped by Atwood and Mather (1932) is an attractive datum to measure the spatial variation of incision into the volcanic field, however, because of concerns about the origin of flat topography that was used to define the peneplain (Steven, 1968) other surfaces would be preferred. Small and Anderson (1998) and Brocklehurst and Whipple (2002) showed how different surfaces could be generated using modern topography and Oskin and Burbank (2005) took advantage of the position of a regional unconformity to measure the variation in incision between different areas or different erosive processes. To create a reliable surface to use for measuring incision and geophysical relief for the San Juan Mountains I attempted a combination of these techniques.

At the close of major volcanism at the beginning of the Miocene there was a distinct change in the chemistry of continued minor eruptions. Bimodal volcanism spread thin, yet aerially extensive basalt flows over much of the volcanic field (Lipman et al., 1978). An attempt was made to take advantage of the modern elevation of outcrops of basalt to measure the extent of post-eruption uplift and incision throughout the range. The theory behind the idea was that the low viscosity of the basaltic magma would allow it to flow into valleys and cool on low angle slopes, thus creating a blanket over the volcanic topography and preserving a sort of base level elevation from early Miocene. This idea did not prove to be effective because of the limited spatial extent of basaltic outcrop in the northwestern portion of the range. Interestingly almost no basalt is left on the west side of the Continental Divide (probably a result of greater exhumation) and though the

lack of it may very well be evidence of greater exhumation in the northwest that is suggested by the thermochronology results, a lack of evidence is not evidence for an idea and therefore the use of a lithologic boundary to measure exhumation and incision was not effective in the San Juan Mountains. Because of this and the questions surrounding the Atwood and Mather Peneplain surface, I settled on using a modeled maximum topography surface to measure incision and geophysical relief. Figure A6 shows how the distribution of incision estimated by using

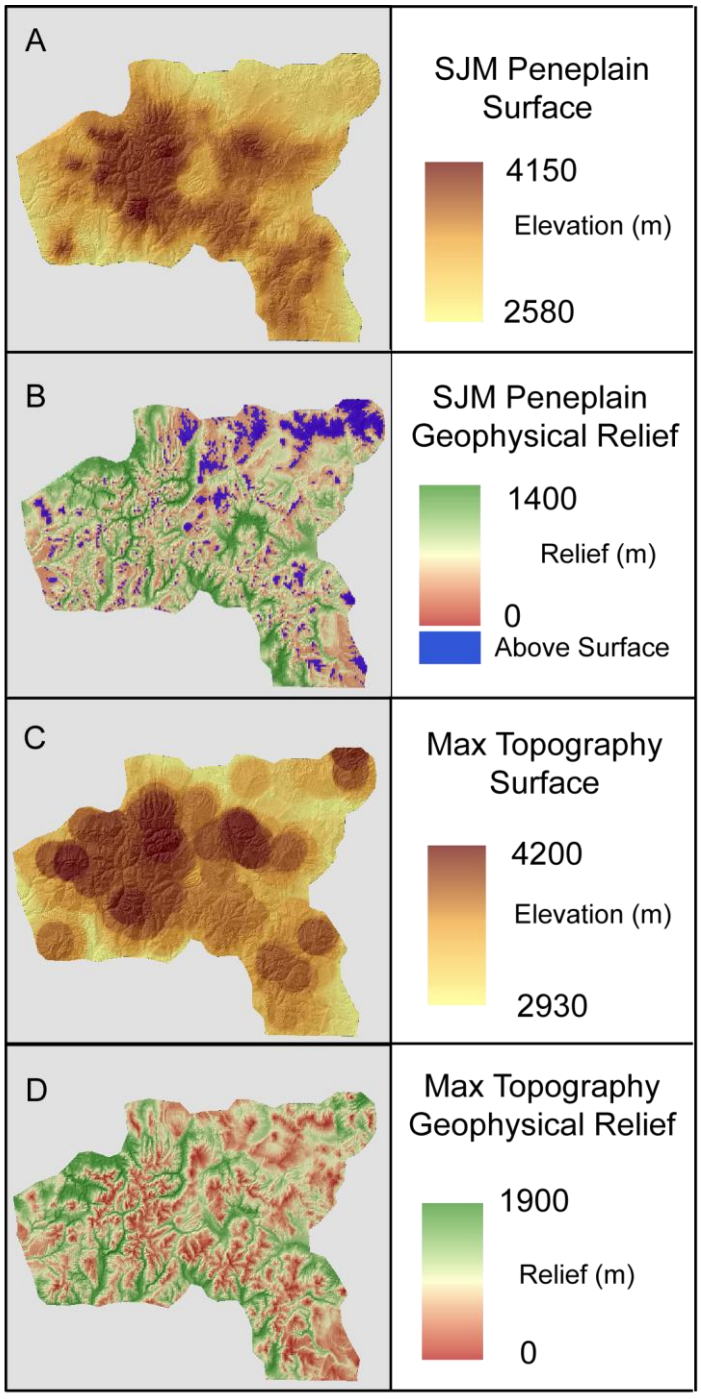

Figure A6. Maps A and C show the elevation of surfaces used to calculate geophysical relief: A) Atwood and Mather's San Juan Peneplain; C) Modeled maximum topography. Maps B and D show the distribution and magnitude of geophysical relief in the San Juan Mountains: B) Relative to the peneplain surface; D) relative to the maximum topography surface.

both the Peneplain surface of Atwood and Mather and the modeled maximum topography surface is quite similar.

APPENDIX D

ADDITIONAL DATA FROM RESULTS

Apatite (U-Th)/He Thermochronology

Table A4. Laboratory Results for San Juan Mountains Apatite (U-Th)/He Analysis
Analyzed by R. McKeon, S. Kelley, and D. Stockli at the University of Kansas

Sample	Age [Ma]	± [Ma]	U [ppm]	Th [ppm]	Sm [ppm]	He [nmol/g]	mass [mg]	Ft	stddev
NWBP1-1	10.9	0.7	13.8	42.5	148.7	0.94	1.9	0.64	
NWBP1-2	8.8	0.5	15.8	39.1	137.2	0.85	2.8	0.68	
NWBP1-3	10.3	0.6	15.4	68.3	177.5	1.11	1.4	0.60	
NWBP1	***10.0***	***0.6***	***15.0***	***50.0***	***154.5***	***0.97***	***2.0***	***0.64***	***1.1***
NWBP4-1	3.6	0.2	15.4	65.5	136.4	0.43	3.9	0.70	
NWBP4-2*	23.0	1.4	24.5	83.3	156.0	3.76	2.5	0.67	
NWBP4-3	4.9	0.3	11.5	31.7	92.2	0.34	4.7	0.66	
NWBP4	***4.2***	***0.3***	***13.5***	***48.6***	***114.3***	***0.4***	***4.3***	***0.68***	***0.9***
NWWS1-1	22.5	1.7	6.8	32.5	136.9	1.02	1.2	0.59	
NWWS1-2	21.4	1.3	4.9	24.6	98.1	0.72	0.8	0.54	
NWWS1-3[1]	-0.6	0.0	-0.4	7.5	3.1	0.00	0.8	0.52	
NWWS1	***21.9***	***1.5***	***5.8***	***28.6***	***117.5***	***0.87***	***1.0***	***0.57***	***0.8***
NWWS4-1	18.6	1.1	13.8	31.7	41.4	1.60	4.9	0.73	
NWWS4-2	19.9	1.2	22.5	57.0	68.3	2.76	3.2	0.70	
NWWS4-3	21.8	1.3	15.8	30.7	60.2	1.68	1.6	0.60	
NWWS4	***20.1***	***1.2***	***17.4***	***39.8***	***56.6***	***2.01***	***3.2***	***0.68***	***1.6***
NWSS1-1	4.7	0.3	5.6	19.4	126.8	0.22	9.0	0.78	
NWSS1-2	5.4	0.3	7.1	18.8	108.6	0.28	9.8	0.78	
NWSS1-3	6.1	0.4	7.8	20.5	105.7	0.36	13.3	0.81	
NWSS1	***5.4***	***0.3***	***6.8***	***19.6***	***113.7***	***0.29***	***10.7***	***0.79***	***0.7***
NWSS2-1	10.9	0.7	7.7	28.3	139.3	0.58	1.7	0.63	
NWSS2-2	7.4	0.4	7.5	24.4	112.9	0.35	1.5	0.61	
NWSS2-3	10.0	0.7	5.3	21.6	133.9	0.42	2.1	0.65	
NWSS2	***9.4***	***0.6***	***6.9***	***24.7***	***128.7***	***0.45***	***1.8***	***0.63***	***1.9***
NWSS3-1*	22.2	1.3	4.0	12.9	111.0	0.64	5.1	0.68	
NWSS3-2	5.7	0.3	5.1	15.5	143.1	0.22	11.6	0.74	
NWSS3-3	5.9	0.4	5.7	18.2	153.7	0.25	7.3	0.70	
NWSS3	***5.8***	***0.3***	***5.4***	***16.8***	***148.4***	***0.24***	***9.5***	***0.72***	***0.1***
NWSS4-1	2.7	0.2	14.4	36.8	68.5	0.25	4.0	0.71	
NWSS4-2	3.2	0.2	12.6	39.8	74.6	0.28	5.1	0.73	
NWSS4-3	2.5	0.1	3.7	6.0	62.9	0.05	2.8	0.68	
NWSS4	***2.8***	***0.2***	***10.2***	***27.5***	***68.7***	***0.19***	***4.0***	***0.71***	***0.3***

Table A4 Continued

NWSS5-1	3.0	0.2	5.6	19.7	90.6	0.13	9.6	0.72	
NWSS5-2	2.5	0.2	4.0	12.3	63.1	0.07	11.2	0.72	
NWSS5-3	3.0	0.2	2.8	7.5	54.5	0.06	7.7	0.72	
NWSS5	***2.8***	***0.2***	***4.1***	***13.2***	***69.4***	***0.09***	***9.5***	***0.72***	***0.3***
PAR1-1	29.4	1.8	5.9	12.1	142.5	0.91	1.0	0.58	
PAR1-2	32.5	1.9	8.1	28.2	177.4	1.66	1.1	0.58	
PAR1-3	22.9	1.4	7.3	32.0	167.2	1.25	2.2	0.62	
PAR1	***28.3***	***1.7***	***7.1***	***24.1***	***162.3***	***1.27***	***1.4***	***0.59***	***4.9***
PAR3-1	26.4	1.6	4.5	13.6	103.3	0.82	5.3	0.67	
PAR3-2	21.0	1.3	18.6	26.4	127.0	2.14	9.5	0.73	
PAR3-3	19.5	1.2	8.1	26.5	110.7	1.20	12.5	0.75	
PAR3	***22.3***	***1.3***	***10.4***	***22.2***	***113.7***	***1.39***	***9.1***	***0.72***	***3.6***
PDC1-1*	61.9	3.7	4.3	9.2	160.3	1.54	1.2	0.59	
PDC1-2	32.5	2.0	2.4	8.6	71.2	0.61	3.1	0.69	
PDC1-3	31.4	1.9	4.5	21.8	144.0	1.22	2.4	0.67	
PDC1	***31.9***	***1.9***	***3.4***	***15.2***	***107.6***	***0.9***	***2.8***	***0.68***	***0.8***
PBC1-1	22.9	1.4	31.4	5.2	145.4	2.80	1.8	0.67	
PBC1-2*	35.9	2.2	11.0	15.0	55.8	1.93	2.0	0.66	
PBC1-3	19.1	1.1	8.4	98.2	113.6	1.94	1.1	0.58	
PBC1	***21.0***	***1.3***	***19.9***	***51.7***	***129.5***	***2.4***	***1.4***	***0.6***	***2.6***
PBC2-1*	35.3	2.1	7.0	1.1	105.9	1.01	1.6	0.65	
PBC2-2	19.2	1.1	30.4	44.2	139.8	2.83	2.0	0.65	
PBC2-3	19.3	1.2	17.5	23.7	114.0	1.48	2.2	0.59	
PBC2	***19.2***	***1.2***	***24.0***	***33.9***	***126.9***	***2.2***	***2.1***	***0.6***	***0.1***

* = Age likely affected by the presence of a zircon inclusion within the apatite grain and not used in age calculation.

[1] = No grain present in Pt tube, lost during packing of grains in Pt tubes prior to Helium extraction.

Northeast-Facing Cirque Data

Table A5. Elevation, relief, and bedrock geology data for all northeast facing cirques

Cirque ID	Swath	Outlet Elevation (m)	Maximum Elevation (m)	Cirque Relief (m)	Bedrock Geology
4	S	3562	3783	221	Volcanic
5	S	3513	3739	226	Volcanic
6	S	3574	3817	243	Volcanic
7	S	3734	3961	227	Volcanic
9	S	3503	3826	323	Volcanic
11	S	3675	3931	256	Volcanic
16	S	3473	3650	177	Volcanic
17	S	3526	3771	245	Volcanic
25	S	3805	4110	305	Volcanic
26	S	3632	3904	272	Volcanic
28	S	3618	3846	228	Volcanic
30	S	3525	3846	321	Volcanic
37	S	3326	3991	665	Volcanic
40	S	3646	3771	125	Volcanic
46	S	3679	4006	327	Volcanic
49	S	3544	3736	192	Volcanic
81	NW	3697	4002	305	Volcanic
82	NW	3809	4174	365	Volcanic
83	NW	3886	4137	251	Volcanic
86	NW	3757	4124	367	Volcanic
89	NW	3904	4275	371	Volcanic
95	NW	3674	4000	326	Precambrian
96	NW	3504	3942	438	Volcanic
97	NW	3597	4018	421	Volcanic
101	NW	3646	4088	442	Volcanic
104	NW	3532	4076	544	Volcanic
108	NW	3749	4094	345	Volcanic
109	NW	3579	4176	597	Volcanic
110	NW	3555	4076	521	Volcanic
112	NW	3708	4146	438	Volcanic
113	NW	3593	4016	423	Precambrian
114	NW	3610	4010	400	Precambrian
115	NW	3704	4028	324	Precambrian
116	NW	3808	4164	356	Precambrian
124	NW	3722	3988	266	Precambrian

Table A5 Continued

126	NW	3630	3960	330	Precambrian
132	NW	3758	4150	392	Precambrian
133	NW	3758	4169	411	Precambrian
134	NW	3733	4141	408	Precambrian
136	NW	3694	4188	494	Precambrian
144	NW	3819	4087	268	Precambrian
146	NW	3667	4281	614	Precambrian
148	NW	3581	4250	669	Precambrian
154	NW	3586	4007	421	Precambrian
155	NW	3635	3979	344	Precambrian
160	NW	3667	3928	261	Precambrian
162	NW	3686	4096	410	Volcanic
164	NW	3538	4090	552	Precambrian
166	NW	3725	4013	288	Volcanic
167	NW	3765	4046	281	Volcanic
170	NW	3597	3962	365	Volcanic
171	NW	3476	4118	642	Volcanic
175	NW	3717	4037	320	Volcanic
176	NW	3427	4087	660	Volcanic
178	NW	3683	4053	370	Volcanic
179	NW	3385	4006	621	Volcanic
182	NW	3587	3961	374	Volcanic
183	NW	3602	3885	283	Volcanic
185	NW	3698	3972	274	Volcanic
187	NW	3466	3947	481	Volcanic
193	NW	3784	4191	407	Volcanic
195	NW	3595	4075	480	Volcanic
196	NW	3423	3934	511	Volcanic
198	NW	3525	4009	484	Volcanic
199	NW	3613	4038	425	Volcanic
205	NW	3655	4047	392	Volcanic
210	NW	3553	4092	539	Volcanic
211	NW	3580	4095	515	Volcanic
213	NW	3707	4171	464	Volcanic
220	NW	3788	4052	264	Volcanic
222	NW	3783	4017	234	Volcanic
226	NW	3454	4209	755	Sedimentary
232	NW	3461	4246	785	Sedimentary
238	NW	3598	4091	493	Volcanic
241	NW	3560	4001	441	Volcanic

Table A5 Continued

242	NW	3796	4093	297	Volcanic
244	NW	3724	4126	402	Volcanic
246	NW	3625	4050	425	Volcanic
249	NW	3537	3954	417	Precambrian
250	NW	3617	3956	339	Precambrian
260	NW	3634	3956	322	Precambrian
261	NW	3619	4163	544	Precambrian
264	NW	3618	4022	404	Sedimentary
267	NW	3420	3735	315	Sedimentary
268	NW	3472	3697	225	Sedimentary

Table A6. Location data for cirques used in the cirque analysis

Cirque ID	Swath	Distance from West Side of Swath (km)	UTM Easting (m)	UTM Northing (m)
4	S	40.93	359536	4127555
5	S	44.14	363056	4127910
6	S	45.82	364609	4127248
7	S	42.54	361711	4128900
9	S	47.29	365903	4126488
11	S	42.28	361786	4129921
16	S	42.28	358414	4120218
17	S	44.52	359419	4116277
25	S	29.14	349792	4135440
26	S	32.84	350602	4126500
28	S	33.18	351470	4127953
30	S	34.00	351267	4124861
37	S	28.09	350046	4139356
40	S	28.83	351372	4140913
46	S	47.30	374094	4150028
49	S	46.15	368921	4138649
81	NW	92.91	297083	4195307
82	NW	87.13	287773	4205970
83	NW	84.19	284650	4206140
86	NW	80.70	281489	4204547
89	NW	78.21	280590	4198981
95	NW	68.65	280330	4167192
96	NW	76.48	287456	4170663
97	NW	71.91	281920	4173130
101	NW	74.75	283636	4177224
104	NW	87.59	292088	4193472
108	NW	83.72	288083	4193311

Table A6 Continued

109	NW	81.73	288107	4186458
110	NW	81.36	287276	4187900
112	NW	85.90	290297	4193529
113	NW	71.63	283853	4165865
114	NW	69.56	281629	4166050
115	NW	68.74	280570	4166720
116	NW	67.97	280216	4165253
124	NW	68.86	277650	4176669
126	NW	70.09	279225	4175705
132	NW	61.50	270521	4174793
133	NW	62.30	271464	4174451
134	NW	60.75	269625	4175167
136	NW	65.01	274952	4172317
144	NW	60.41	270479	4171211
146	NW	61.56	272592	4168244
148	NW	61.81	273087	4167485
154	NW	50.86	260347	4171674
155	NW	54.97	263402	4175740
160	NW	65.75	272371	4183264
162	NW	64.81	270537	4186034
164	NW	65.51	271826	4184220
166	NW	70.95	275896	4189496
167	NW	70.48	275260	4189974
170	NW	68.22	271565	4194317
171	NW	66.80	270122	4194194
175	NW	63.36	268816	4186700
176	NW	64.31	267417	4194508
178	NW	57.17	262944	4184748
179	NW	57.62	262861	4186565
182	NW	53.22	258850	4184621
183	NW	54.82	259723	4187241
185	NW	55.61	258542	4193789
187	NW	51.69	256910	4185726
193	NW	49.70	254021	4188357
195	NW	51.82	255460	4190902
196	NW	46.93	250070	4191803
198	NW	53.21	257112	4190266
199	NW	45.58	250890	4184516
205	NW	68.19	270869	4196491
210	NW	70.87	272461	4200432
211	NW	70.43	271754	4201239
213	NW	77.08	277766	4204326

Table A6 Continued

220	NW	67.40	268614	4201149
222	NW	62.55	262512	4204496
226	NW	37.17	239579	4192737
232	NW	36.48	237967	4195619
238	NW	54.53	255838	4198926
241	NW	54.55	255609	4199733
242	NW	49.96	251857	4196307
244	NW	52.81	254306	4198057
246	NW	58.17	257211	4206859
249	NW	51.81	263789	4163696
250	NW	52.02	264350	4162574
260	NW	65.89	278121	4164972
261	NW	67.01	279180	4165352
264	NW	12.53	227279	4148760
267	NW	13.99	228548	4149602
268	NW	18.41	232290	4152502

REFERENCES CITED

Amerson, B.E., Montgomery, D.R., Meyer, G., 2008, Relative size of fluvial and glaciated valleys in central Idaho. Geomorphology, 93, 537-547.

Andrews, J.T., 1972, Glacier power, mass balances, velocities, and erosional potential. Zietschrift für Geomorphologie. 13, 1-17.

Atwood, W.W., Mather, K.F., 1932, Physiography and Quaternary geology of the San Juan Mountains, Colorado. USGS Professional Paper 166. 176 pp.

Bagnold, R.A., 1960, Flow resistance in sinuous or irregular channels: Part 2. a theoretical model of energy loss in curved channels. USGS Professional Paper, 122-130.

Bartlein, P.J., Anderson, K.H., Anderson, P.M., Edwards, M.E., Mock, C.J., Thompson, R.S., Webb, R.S., Webb III, T., Whitlock, C., 1998, Paleoclimate simulations for North America over the past 21,000 years: Features of the simulated climate and comparisons with paleoenvironmental data. Quaternary Science Reviews, 17, 549-585.

Bishop, M.P., Shroder, J.F., Bonk, R., Olsenholler, J., 2002, Geomorphic change in high mountains: a western Himalayan perspective. Global and Planetary Change 32, 311-329.

Bove, D.J, Hon, K., Budding, K.E., Slack, J.F., Snee, L.W., Yeoman, R.A., 2001, Geochronology and geology of late Oligocene through Miocene volcanism and minerialization in the western San Juan Mountains, Colorado. USGS Professional Paper 1642.

Brocklehurst, S.H., Whipple, K.X., 2002, Glacial erosion and relief production in the eastern Sierra Nevada, California. Geomorphology 42, 1-24.

Brocklehurst, S.H., Whipple, K.X., 2006, Assessing the relative efficiency of fluvial and glacial erosion through simulation of fluvial landscapes. Geomorphology, 75, 283-299.

Broecker, W.S. Denton, G.H., 1990, What drives glacial cycles? Scientific American, 262, 48-56.

Brozovic, N., Burbank, D.W., Meigs, A.J., 1997, Climatic limits on landscape development in the northwestern Himalaya. Science 276, 571-574.

Burbank, D.W., Blythe, A.E., Putkonen, J., Pratt-Sitaula, B., Gabet, E., Oskin, M., Barros, A., Ojha, T.P., 2003, Decoupling of erosion and precipitation in the Himalayas. Nature 426, 652-655.

Clift, P., 2006, Controls on the erosion of Cenozoic Asia and the flux of clastic sediment to the ocean. Earth and Planetary Science Letters, 241, 571-580.

Coblentz, D.D., and van Wijk, J., 2007, Mechanisms of topographic uplift for the Southern Rocky Mountains., Eos Transactions. American Geophysical Union, 88(52), Fall Meeting Supplement, Abstract T11C-0723.

Davis, D., Suppe, J., Dahlen, F.A., 1983, Mechanics of fold-and-thrust belts and accretionary wedges. Journal of Geophysical Research, 88, B2, 1153-1172.

Daly, C., Gibson, W.P., Taylor, G.H., Johnson, G.J., Pasteris, P., 2002, A knowledge-based approach to the statistical mapping of climate. Climate Research, 22, 99-113.

Dueker, K., Yuan, H., Zurek, B., 2001, Thick-structured Proterozoic lithosphere of the Rocky Mountain region. GSA Today 11, 4-9.

Ehlers, T.A., Farley, K.A., 2003, Apatite (U-Th)/He thermochronometry: methods and applications to problems in tectonic and surface processes. Earth and Planetary Science Letters, 206, 1-14.

Epis, R.C., and Chapin, C.E., 1975, Geomorphic and tectonic implications of the post-Laramide late Eocene erosion surface in the southern Rocky Mountains, in Curtis, B.F., ed., Cenozoic history of the southern Rocky Mountains: Geological Society of America Memoir 144, 45-74.

Farley, K.A., 2000, Helium diffusion from apatite: General behavior as illustrated by Durango fluorapatite. Journal of Geophysical Research, 105, 2903-2914.

Foster, D., Brocklehurst, S.H., Gawthorpe, R.L., 2008, Small valley glaciers and the effectiveness of the glacial buzzsaw in the northern Basin and Range, USA. Geomorphology, 102, 632-639.

Green, Gregory N. , 1992, The Digital Geologic Map of Colorado in ARC/INFO Format: U.S. Geological Survey Open-File Report 92-507, U.S. Geological Survey, Denver.

Gregory, K.M., Chase, C.G., 1992, Tectonic significance of paleobotanically estimated climate and altitude of the late Eocene erosion surface, Colorado. Geology, 20, 581-585.

Hallet, B., Hunter, L., Bogen, J., 1996, Rates of erosion and sediment evacuation by glaciers: a review of field data and their implications. Global and Planetary Change 12, 213-235.

Harbor, J., Washburton, J., 1993. Relative rates of glacial and nonglacial erosion in alpine environments. Arctic Alpine Res. 25, 1-7.

Hicks, D., Murray, M., McSaveney, J., Chinn, T.J.H., 1990, Sedimentation in proglacial Ivory Lake, Southern Alps, New Zealand. Arctic Alpine Research. 22, 26-42.

Humlum, O., 1986, Mapping of glaciation levels: Comments on the effect of sampling area size. Arctic and Alpine Research, 18, 407-414.

Karlstrom, K.E., Whitmeyer, S.J., Dueker, K., Williams, M.L., Bowring, S.A., Levander, A., Humphreys, E.D., Keller, G.R., CD-ROM Working Group, 2005, Synthesis of results from the CD-ROM experiment: 4-D image of the lithosphere beneath the Rocky Mountains and implications for understanding the evolution of continental lithosphere: in The Rocky Mountain region: Evolving lithosphere tectonics, geochemistry, and geophysics, American Geophysical Union Monograph 154, 421-441.

Karlstrom, K.E., Project, C., 2007, Interconnections Between the Mantle and the Near-Surface System Above the Aspen Anomaly, Central Colorado, and Implications for Cenozoic Uplift of the Rocky Mountains. Eos Transactions. American Geophysical Union, 88(52), Fall Meeting Supplement, Abstract T14C-02.

Kellogg, K.S., 1999, Neogene basins of the northern Rio Grande rift: partitioning and asymmetry inherited from Laramide and older uplifts. Tectonophysics 305, 141-152.

Ketcham, R.A., Donelick, R.A., Carlson, W.D., 1999, Variability of apatite fission-track annealing kinetics: III extrapolation to geologic time scales. American Mineralogist, 84, 1235-1255.

Koppes, M.N., Hallet, B., 2002, Influence of rapid glacial retreat on the rate of erosion by tidewater glaciers. Geology 30, 47-50.

Laslett, G.M., Green, P.F., Duddy, I.R., Gleadow, A.J.W., 1987, Thermal annealing of fission tracks in apatite. 2. A quantitative analysis. Chemical Geology, 65, 1-13.

Leonard, E.M., 1984, Late Pleistocene equilibrium-line altitudes and modern snow accumulation patterns, San Juan Mountains, Colorado, USA. Arctic and Alpine Research 16, 65-76.

Leonard, E.M., 2002, Geomorphic and tectonic forcing of late Cenozoic warping of the Colorado piedmont: Geology, v. 30, 595-598.

Lipman, P.W., Doe, B.R., Hedge, C.E., Steven, T.A., 1978, Petrologic evolution of the San Juan volcanic field, southwestern Colorado: Pb and Sr isotope evidence. GSA Bulletin, 89, 59-82.

McMillan, M.E., Heller, P.L., Wing, S.L., 2006, History and causes of post-Laramide relief in the Rocky Mountain orogenic plateau. GSA Bulletin, 118, 393-405.

Meigs, A., Sauber, J., 2000, Southeast Alaska as an example of the long-term consequences of mountain building under the influence of glaciers. Quat. Sci. Rev. 19, 1543-1562.

Mitchell S.G., Montgomery, D.R., 2006, Influence of a glacial buzzsaw on the height and morphology of the Cascade Range in central Washington State, USA. Quaternary Research 65, 96-107.

Mitchell, S.G., Reiners, P.W., 2003, Influence of wildfires on apatite and zircon (u-Th)/He ages. Geology, 31, 1025-1028.

Molnar, P. and England, P., 1990, Late Cenozoic Uplift of Mountain Ranges and Global Climate Change: Chicken or Egg?. Nature 346, 29-34.

Mock, C.J., 1996, Climatic controls and spatial variations of precipitation in the western United States. Journal of Climate, 9, 1111-1125.

Montgomery, D.R., 2002, Valley formation by fluvial and glacial erosion. Geology 30, 1047-1050.

Montgomery, D.R., Balco, G., Willett, S.D., 2001, Climate, tectonics, and the morphology of the Andes. Geology 29, 579-582.

Morgan, Paul, pers. comm. 2008, Denver Museum of Nature and Science, paul.morgan@dmns.org.

Morgan, P., Seager, W.R., Golombek, M.P., 1986, Cenozoic thermal, mechanical, and tectonic evolution of the Rio Grande Rift. Journal of Geophysical Research, 91, 6263-6276.

Moucha, R., Forte, A.M., Rowley, R.B., Mitrovica, J.X., Simmons, N.A., Grand, S.P., 2008, Mante convection and the recent evolution of the Colorado Plateau and the Rio Grande Rift valley. Geology, 36, 439-442.

Naylor, S., Gabet, E.J., 2007, Valley asymmetry and glacial versus nonglacial erosion in the Bitterroot Range, Montana, USA. Geology 35, 375-378.

Oskin, M., Burbank, D.W., 2005, Alpine landscape evolution dominated by cirque retreat. Geology 33, 933-936.

Porter, S.C., 1989, Some Geological Implications of Average Quaternary Glacial Conditions. Quaternary Research, 32, 245-261.

Porter, S.C. Pierce, K.L., Hamilton, T.D., 1983, Late Pleistocene mountain glaciation in western United States. In: Porter, S.C. (Ed.), Late-Quaternary environments of the United States. Volume I, the late Pleistocene. University of Minnesota Press, Minneapolis, 71-111.

Raymo, M.E., Ruddiman, W.F., 1992, Tectonic forcing of late Cenozoic climate. Nature 359, 117-122.

Reiners, P.W., Ehlers, T.A., Mitchell, S.G., Montgomery, D.R., 2003, Coupled spatial variations in precipitation and long-term erosion rates across the Washington Cascades. Nature 426, 645-647.

Reusser, L.J., Bierman, P.R., Pavich, M.J., Zen, E., Larsen, J., Finkel, R., 2004, Rapid late Pleistocene incision of Atlantic passive-margin river gorges. Science 305, 499-502.

Roy, M., Kelley, S., Pazzaglia, F.J., Cather, S., and House, M.A., 2004, Middle Tertiary buoyancy modification and its relationship to rock exhumation, cooling, and subsequent extension at the eastern margin of the Colorado Plateau; Geology, v. 32, 925-928.

Sheppard, P.R., Comrie, A.C., Packin, G.D., Angersbach, K., Hughes, M.K., 2002, The climate of the US Southwest. Climate Research, 21, 219-238.

Small, E.E., Anderson, R.S., 1998, Pleistocene relief production in Laramide mountain ranges, western United States. Geology, 26, 123-126.

Spotila, J.A., Buscher, J.T., Meigs, A.J., Reiners, P.W., 2004, Long-term glacial erosion of active mountain belts: Example of the Chugach-St.Elias Range, Alaska. Geology 32, 501-504.

Steven, T.A., 1968, Critical review of the San Juan Peneplain, southwestern Colorado. USGS Professional Paper 594-I, 19 pp.

Steven, T.A., Lipman, P.W., 1976, Calderas of the San Juan volcanic field, southwestern Colorado. USGS Professional Paper 958, 35 pp.

Steven, T.A., Hon, K., Lanphere, M.A., 1995. Neogene geomorphic evolution of the central San Juan Mountains near Creede, Colorado. Miscellaneous Investigations Series I-2504, USGS.

Stockli, D.F., Farley, K.A., Dumitru, T.A., 2000, Calibration of the apatite (U-Th)/He thermochronometer on an exhumed fault block, White Mountains, California. Geology, 28, 983-986.

Thomson, S.N., 2002. Late Cenozoic geomorphic and tectonic evolution of the Patagonian Andes between latitudes 42˚S and 46˚S: An appraisal based on fission-track results from the transpressional intra Liquiñe-Ofqui fault zone. GSA Bulletin, 114, #9, 1159-1173.

Tomkin, J.H., Braun, J., 2002. The influence of alpine glaciation on the relief of tectonically active mountain belts. Am. J. Sci. 302, 169-190.

West, M., Ni, J., Baldridge, W.S., Wilson, D., Aster, R., Gao, W., Grand, S., 2004, Crust and upper mantle shear wave structure of the Southwest United States: Implications for rifting and support for high elevation. Journal of Geophysical Research, 109, B03309.

Whipple, K.X., Kirby, E., Brocklehurst, S.H., 1999. Geomorphic limits to climate-induced increases in topographic relief. Nature 401, 39-43.

Willett, S.D., 1999. Orogeny and orography: The effects of erosion on the structure of mountain belts. Journal of Geophysical Research 104, 28,957-28,981.